Dental Materials 39 (2023) 539–556

Contents lists available at ScienceDirect

Dental Materials

journal homepage: www.elsevier.com/locate/dental

Finite element analysis in implant dentistry: State of the art and future directions

Cristina Falcinelli[a,*,1], Francesco Valente[b,c,1], Marcello Vasta[a], Tonino Traini[b,c]

[a] Department of Engineering and Geology, University "G. d'Annunzio" of Chieti-Pescara, Viale Pindaro 42, Pescara 65127, Italy
[b] Department of Innovative Technologies in Medicine & Dentistry, University "G. d'Annunzio" of Chieti-Pescara, Via dei Vestini 31, Chieti 66100, Italy
[c] Electron Microscopy Laboratory, University "G. d'Annunzio" of Chieti-Pescara, Via dei Vestini 31, Chieti 66100, Italy

ARTICLE INFO

Keywords:
Dental implants
Finite element modeling and analysis
Bone-implant interface
Osseointegration
Bone remodeling

ABSTRACT

Objective: To discuss the state of the art of Finite Element (FE) modeling in implant dentistry, to highlight the principal features and the current limitations, and giving recommendations to pave the way for future studies.
Methods: The articles' search was performed through PubMed, Web of Science, Scopus, Science Direct, and Google Scholar using specific keywords. The articles were selected based on the inclusion and exclusion criteria, after title, abstract and full-text evaluation. A total of 147 studies were included in this review.
Results: To date, the FE analysis of the bone-dental implant system has been investigated by analyzing several types of implants; modeling only a portion of bone considered as isotropic material, despite its anisotropic behavior; assuming in most cases complete osseointegration; considering compressive or oblique forces acting on the implant; neglecting muscle forces and the bone remodeling process. Finally, there is no standardized approach for FE modeling in the dentistry field.
Significance: FE modeling is an effective computational tool to investigate the long-term stability of implants. The ultimate aim is to transfer such technology into clinical practice to help dentists in the diagnostic and therapeutic phases. To do this, future research should deeply investigate the loading influence on the bone-implant complex at a microscale level. This is a key factor still not adequately studied. Thus, a multiscale model could be useful, allowing to account for this information through multiple length scales. It could help to obtain information about the relationship among implant design, distribution of bone stress, and bone growth. Finally, the adoption of a standardized approach will be necessary, in order to make FE modeling highly predictive of the implant's long-term stability.

1. Introduction

1.1. Background

The finite element (FE) method is a numerical technique that is used to analyze and simulate physical phenomena. It is commonly used in product design to reduce the need for physical prototypes and experiments and to optimize components in order to create better products more efficiently and cost-effectively. The FE method relies on mathematical models to understand and quantify various physical phenomena, including structural and fluid behavior, mechanical stress, thermal transport, wave propagation, and the growth of biological cells [1]. The FE method has become an increasingly useful tool due to technological development and also has great growth prospects for the future: the Global Simulation & Analysis Software Market size was estimated at USD 18.25 billion in 2022, and is projected to grow at a compound annual growth rate of 14.92% to reach USD 36.68 billion by 2027.

In the medical field, the FE method is particularly useful for studying complex biomechanical systems that are difficult to study in-vivo or in-vitro. It can be used to predict the mechanical response of tissues under different stimulation conditions, both in healthy and pathological states, and to assess the structural changes [2–4]. Moreover, the FE method has been also extensively used during medical device design, allowing for the investigation of function and possible complications of novel devices [5].

Over the years a large amount of research has been carried out on the application of the FE method in dentistry [6]. Most of the research has been focused on examining the implant mechanical behavior during functional loads with the aim to assess the stress and strain fields in

* Corresponding author.
E-mail address: cristina.falcinelli@unich.it (C. Falcinelli).
[1] These authors equally contributed to this work.

https://doi.org/10.1016/j.dental.2023.04.002
Received 12 January 2023; Received in revised form 30 March 2023; Accepted 5 April 2023

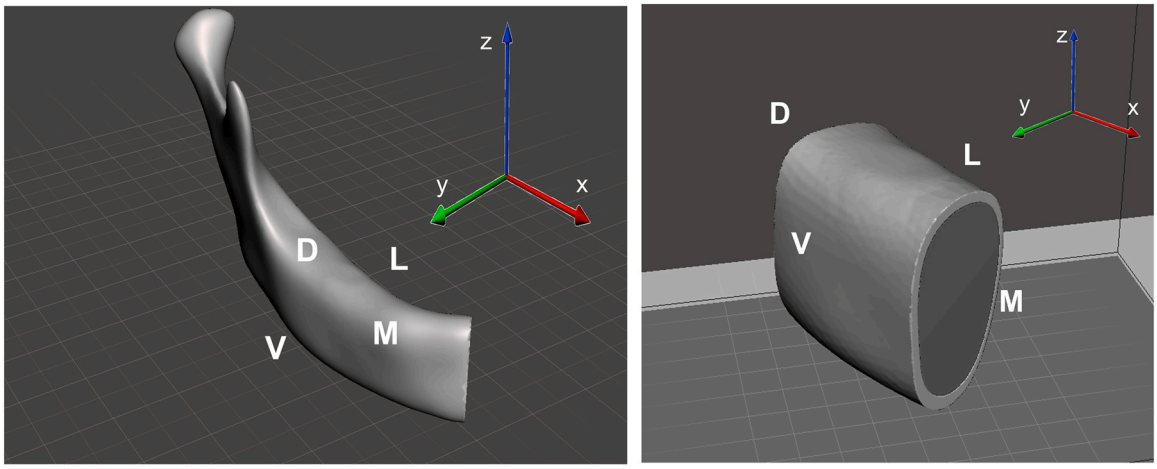

Fig. 1. (a) A right mandible is shown with the specification of mesial (M), distal (D), vestibular (V) and lingual (L) directions. (b) Bone segment extracted from a right mandible with the specification of mesial (M), distal (D), vestibular (V) and lingual (L) directions. The bone segment is composed of an inner portion that corresponds to the trabecular bone (dark grey) and an external portion that represents the cortical layer (light grey).

implant components and bone at a macroscale level [7,8]. However, mechanical loading induces adaptive changes at a microscale level affecting bone homeostasis and remodeling. These changes significantly impact the shape of the stress and strain fields at the bone-implant interface [9–11]. Capturing these effects through numerical modeling may open a new wave of multidisciplinary approaches aiming to understand and control biointegration and improve the long-term survival of dental implants.

1.2. Aim

This review aims to provide a comprehensive overview of the FE method application in implant dentistry. All the main aspects are discussed, with the intent to give recommendations to overcome the current limitations. Finally, an examination of future perspectives is provided.

1.3. Literature search

The electronic search was conducted through Pubmed, Web of Science, Scopus, Science Direct, and Google Scholar. The aim was to investigate the mechanical response of bone-dental implant systems. The following keywords have been used: “dental implant”, “finite element analysis”, “finite element modeling”, “bone-dental implant interface”, “osseointegration”, and “bone remodeling”. Inclusion criteria were full papers (in-silico, in-vitro and in-vivo studies and any kind of review) and conference proceedings published in English within the last twenty years that are focused on FE analysis and bone properties. Exclusion criteria were no dental application and publication in a language other than English. The articles were selected based on their title and abstract, and then the full text was evaluated to identify studies that passed the inclusion and exclusion criteria. A total of 147 studies were included in this review.

1.4. Outline

The review is organized in the following way. Section 2 furnishes a critical and detailed overview of the FE modeling and analysis to study the mechanical behavior of dental implants. In detail, all aspects involved in FE modeling and analysis are examined and in particular: geometry (Section 2.1), computational discretization (Section 2.2), constitutive behavior (Section 2.3), bone remodeling (Section 2.3), bone-implant interface (Section 2.5), and loading and boundary conditions (Section 2.6). In addition, an overview of the main FE outcomes is provided in Section 2.7. In Section 3, the current knowledge about the influence of load on dental implants’ stability and bone response is provided. The way this key factor could be further interpreted to bring the FE analysis to the “next step” is discussed. Finally, suggestions to overcome the current limitations in the FE modeling are given in Section 4.

2. FE modeling and analysis of dental implant-bone systems

In the following, the main steps of FE modeling and analysis of dental implant-bone systems are investigated in detail, with the aim to furnish a comprehensive overview of the main aspects and the principal outcomes. It is also discussed which questions are still open.

For a better understanding, the anatomical and geometric terminologies used in the following are reported in Figs. 1 and 2. In particular, Fig. 1(a) shows a portion of a right mandible from which the bone segment reported in Fig. 1(b) has been extracted. The mesial, distal, vestibular, and lingual directions are reported in Fig. 1. Fig. 2 shows the dental implant with its parts. In general, a dental implant for the rehabilitation of a single tooth consists of the body implant (the fixture, that is inserted into the bone), the abutment, the connection between the fixture and the abutment, and the prosthetic crown (Fig. 2(a)). The anatomy of the connection varies. Its anti-rotational device geometry can be hexagonal, octagonal, trilobate, or others. The connection can be screw-retained, conometric, or cemented. Depending on the materials selected for fabrication, the crown can be either monolithic or it is composed of a framework and an external superstructure (for example metal-ceramic crowns). The dental crown can be cemented on the abutment, or it can be directly connected to the fixture with a passing screw. In the latter, the crown has a hole on its surface allowing access to the passing screw. Fig. 2(b) shows the implant inserted into the bone segment.

2.1. Geometry

The first step to generate a FE model is the geometry representation. In the following, bone and implant geometries are analyzed in detail.

2.1.1. Bone geometry

The reconstructed bone geometry can be classified as simplified geometry and image-based geometry.

In the context of a simplified geometry, bone has been modeled as a two-dimensional (2D) or three-dimensional (3D) object with different

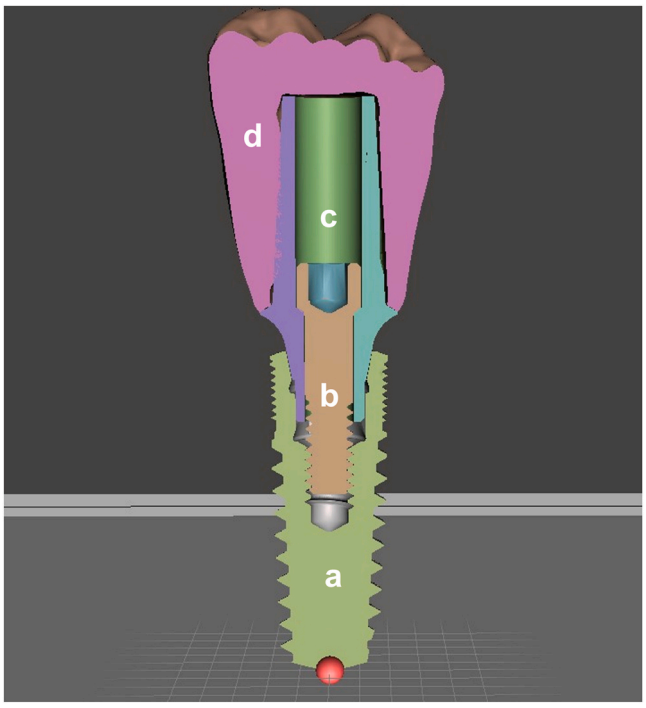

Fig. 2. (a) The main parts of a dental implant are shown: a. body implant; b. passing screw; c. abutment; d. crown. (b) The dental implant inserted into a bone segment.

shapes as shown in Table 1[12–15–18–21–24–27–30–33–36–39].

Even if a simplified shape has been used, the geometry accounts for cortical and trabecular parts. In general, a core of trabecular bone is located in the inner portion and it is surrounded by a cortical shell with a thickness that ranges from 0.5 mm to 3 mm. In the context of accounting for cortical and trabecular bone, in some studies, different bone qualities have been investigated based on the classification of Lekholm & Zarb [40], which is widely adopted in implant dentistry. This is a qualitative classification, and defines four bone types (D_1, D_2, D_3, and D_4) based on the relationship between cortical and trabecular bones. D_1 is characterized by a homogeneous compact bone, whereas D_2 is composed of a thick layer of compact bone surrounding a core of dense trabecular bone. D_3 refers to a thin layer of cortical bone surrounding dense trabecular bone, and D_4 corresponds to a thin layer of cortical bone surrounding a core of low-density trabecular bone. Based on the type of bone to investigate, different values of cortical thickness are used in the geometry, as reported in Table 1.

Instead of reconstructing a simplified geometry, due to the development of digital imaging techniques, in some works, the geometry has been derived from diagnostic image data such as Computed Tomography (CT), allowing a more realistic reconstruction [41–44–47–50–53–56–59–62,63,64].

Both in the case of a simplified geometry and a geometry reconstructed from CT images, bone is modeled as a continuum material, disregarding the trabecular network. However bone failure and adaptation processes are phenomena that occur at the level of individual trabecula. As such, considering the detailed trabecular architecture has been demonstrated to be a key factor to assess stress and strain at the bone-implant interface, thus evaluating the implant stability and its success [65,66]. The organization of the trabecular network can be derived from micro-CT images that allow the generation of FE models that account for the fine organization of trabecular bone. Marcian et al. [67,68] used micro-CT-derived FE models to assess the micro-strain and displacement induced by loaded dental implants at different stages of osseointegration considering different implant geometries. They demonstrated that strain distribution is highly dependent on the architecture of trabecular bone and showed that partial osseointegration is a potential risk of implant longevity. The importance of considering the complex trabecular architecture in FE models was also demonstrated in [69–71], showing that the omission of such an aspect can significantly affect simulations of bone-implant performances. Even if micro-CT images offer the possibility to obtain complex computational models of trabecular bone, in view of the application of FE models in clinical routine micro-CT scanning cannot be carried out on living patients due to high-dose radiation exposure. As such, combining the diagnostic images acquired with clinical settings with deblurring algorithms [72,73] that reduce the partial volume artifacts of clinical images and restore the intensity data could help to detect the trabecular architecture to include in the FE models and thus be a solution to the aforementioned problem. This needs to be deeply investigated in dentistry and may provide new insight into the complex bone strain distribution pattern, that to date has been left underestimated.

2.1.2. Implant geometry

The dental implant geometry is in general derived from 3D computer-aided design data that can be provided by the manufacturers. Table 2 furnishes an overview of the dental implants that have been analyzed in the works reported in the literature. The manufacturer, name of the implant, its parts, and geometric characteristics are reported. As shown in Table 2, different types of implants from different manufacturers and characterized by different geometric features have been investigated, demonstrating a wide variability. Moreover, dental implants are not homogeneous in terms of components that characterize each implant. Implant geometry is an important factor in evaluating stress and strain at the bone-implant interface. In fact, when the surrounding bone is subjected to remodeling, the geometric characteristics may influence implant performance, intensifying the bone loss [69]. From Table 2, it can be observed that the type of connection between the abutment and body implant is another important factor to be considered for investigating the mechanical response. It affects the force transmission mechanism at the body implant-abutment and bone-implant interface [74]. It has been reported that the taper-integrated screwed-in connection leads to a great amount of bone resorption due to large overload [74].

The implant geometry plays an important role in influencing peri-implant bone response. Moreover, it is essential to design patient-specific and site-specific dental implants. The goal should be to make them compatible with the conditions of the patient's bone to create a biomechanical environment that will aid osseointegration at the bone-implant interface. As such, it is essential to address further research toward developing numerical modeling that accounting for patient-specific bone conditions can help in designing personalized and site-specific dental implants. In this context, 3D additive manufacturing can be considered useful for manufacturing patient-specific and site-specific implants enabling relatively easy fabrication of complex implants at low costs.

2.2. Computational discretization

The subsequent step in generating the FE model is the computational discretization of bone and dental implants, namely the mesh generation. For bone and dental implants, hexahedral elements [14,20,26] and linear or quadratic tetrahedral elements [17,23,24,25,27,28,35,38,42,50,54,56,64,75–78–81–84,85] have been employed. In most cases, tetrahedral elements are used. This is related to their capacity to better fit complex geometries [86]. In general, the choice of element type (linear or quadratic) and thus shape function is problem dependent. Quadratic elements admit a parabolic displacement field over each element enabling stress and strain to vary linearly over each element and thus allowing to better capture stress and strain gradients within the single element. Conversely, individual linear elements exhibit a constant value of strain and stress. Moreover, quadratic elements are able to capture more accurately geometric curvature allowing a better representation of the geometry. However, higher order

Table 1
Main characteristics of simplified geometries used for bone. NR: not reported; COR: cortical bone; TRAB: trabecular bone; *h*: height; *l*: length in mesiodistal direction; *w*: width in buccolingual direction; D_1, D_2, D_3 and D_4 refer to the Lekholm & Zarb [40] classification that defines four bone types based on the relationship between cortical and trabecular bones.

Reference	Bone geometry	Characteristics
Chun et al.[13]	2D rectangle $20(h) \times 16(l)$ mm^2	only COR
Huang et al.[14]	3D block $10 \times 10 \times 15$ mm^3	only COR for D_1; COR of 1.2–1.6 mm in thickness for D_2 dense TRAB in the inner portion; COR of 0.6–0.8 mm in thickness for D_3 dense TRAB in the inner portion; COR of 0.6–0.8 mm in thickness for D_4 loose TRAB in the inner part
Mellal et al.[15]	3D block $20(h) \times 10(w) \times 30(l)$ mm^3	COR of 1 mm in thickness TRAB in the inner portion
Lin et al.[17]	3D block $24(h) \times 12(w) \times 15(l)$ mm^3	COR of 1.5 mm in thickness TRAB in the inner portion
Kitagawa et al.[18]	3D block $24.5(h) \times 12.5(w) \times 10(l)$ mm^3	COR and TRAB modeled COR thicknesses: 1.0 mm mandibular superior border, 2.5 mm buccal border, 2.0 mm lingual border, 3.0 mm mandibular inferior border
Sevimay et al.[19]	3D block 24.2(h) mm, 16.3(w) mm	COR and TRAB modeled D_1, D_2, D_3 and D_4 bone types modeled
Heckmann et al.[20]	3D block	COR and TRAB modeled, thickness values of COR NR
Akca et al.[21]	3D cylinder (13 mm height)	COR of 1 mm in thickness TRAB with 12 mm height
Kurniawan et al.[22]	3D block	COR of 2, 1 and 1 mm for D_2, D_3 and D_4 bone types, respectively; TRAB in the inner portion with a density high for D_2 and D_3 bone types, and low for D_4 bone
Tian et al.[23]	3D block $20(h) \times 9(w) \times 20(l)$ mm^3	COR of 1.5 mm in thickness TRAB in the inner portion
Chang et al.[24]	3D cuboid $20(h) \times 10(w) \times 10(l)$ mm^3	COR of 2 mm in thickness for D_2 bone type dense TRAB in the inner portion; COR of 1 mm in thickness for D_4 bone type loose TRAB in the inner portion
Wu et al.[25]	3D block $43.5(h) \times 30(w) \times 41(l)$ mm^3	COR of 3 mm in thickness in the upper part of the 3D block TRAB below the layer of COR
Ueda et al.[26]	3D block	COR of six different thickness values (range 0.5–2 mm) TRAB in the inner portion
Poovarodom et al.[27]	3D block $12.5(h) \times 7.6(w) \times 10(l)$ mm^3	COR of 2 mm in thickness TRAB in the inner portion
Ozturk et al.[28]	3D block $20(h) \times 20(w) \times 20(l)$ mm^3	COR of 1.5 mm in thickness TRAB in the inner portion
Dhatrak et al.[29]	3D block $30(h) \times 10(w) \times 20(l)$ mm^3	COR of 2 mm in thickness TRAB in the inner portion
Shash et al.[30]	3D block $20(h) \times 15(w) \times 15(l)$ mm^3	COR of 2 mm in thickness TRAB in the inner portion
Oliveira et al.[31]	3D block	COR of three different thickness values (0.5, 1 and 2 mm) TRAB in the inner portion with a density at two levels (high and low)
Badalia et al.[32]	3D shape	COR of 1.5 mm in thickness TRAB in the inner portion
Wu et al.[33]	3D block $25(h) \times 12(w) \times 10(l)$ mm^3	COR of 2 mm in thickness TRAB in the inner portion
Paracchini et al.[34]	3D block 17 mm (h) and 12 mm (w)	COR of 2 mm in thickness TRAB in the inner portion
Nokar et al.[35]	3D block $25(h) \times 23(l)$	COR of 2 mm in thickness TRAB in the inner portion
Dhatrak et al.[36]	3D block	COR and TRAB modeled thickness value of COR NR
Barbosa et al.[37]	3D block	COR of 1 mm in thickness TRAB in the inner portion
Alemayehu et al.[38]	3D block	COR and TRAB modeled thickness value of COR NR
Milone et al.[39]	3D block	COR and TRAB modeled thickness value of COR NR

Table 2
Overview of dental implants analyzed in different studies. NR: not reported; A: abutment; BI: body implant; S: screw; C: crown (CF crown framework, PS prosthetic superstructure); D: diameter; L: length; TL: thread length; TP: thread pitch; TD: thread depth; P: pitch; D_1: lower diameter; D_2: great diameter; DBT: distance between the threads; L_{tot}: implant total length; d: implant maximum diameter; l_{BI}: bone-implant interface length.

Reference	Manufacturer of implant	Name of implant	Implant parts	Geometric characteristics (mm)	Remarks
Sevimay et al.[19]	Straumann	ITI	A, BI, C (CF + PS)	D = 4.1; L = 10	–
Akca et al.[21]	Straumann	Straumann dental implant	A, BI	BI: D = 4.1 & L = 10	–
Kurniawan et al.[22]	NR	NR	A, BI	BI D = 3.8 & L = 10	–
Tian et al.[23]	NR	NR	A, BI	D = 4.1; L = 10	Four dental implant models straight BI connected to a straight A straight BI connected to an angled A angled BI connected to a straight A angled BI connected to an angled A
Chang et al.[24]	NobelBiocare	NobelBiocare MK III tissue-leveled	A, BI, S, C	BI L = 11.5; A L = 7.5 & D = 4.1	–
	Straumann	NobelBiocare bone-leveled		BI L = 10; A L = 6.5 & D = 3.4	
		Straumann SLA bone-leveled		BI L = 10; A L = 6 & D = 3.5	
		Straumann SLA tissue-leveled		BI L = 10; A L = 6 & D = 4.5	
Ozturk et al.[28]	Biohorizon's	Internal Implant	A, BI, S, C (CF + PS)	D = 4; L = 12	A connections designs: Internal Hex
	Camlog	Screw-line K-Series		D = 4.3; L = 13	Tube-in-Tube
	Straumann	Bone level		D = 4.1; L = 12	CrossFit
	Zimmer Biomet	Tapered screw-vent		D = 4.1; L = 13	Fricion-Fit
Dhatrak et al.[29]	NR	Nobel Ankylos Biohorizon Xive	A, BI, S, C	BI D = 3.5 & L = 15	–
Oliveira et al.[31]	SOADCO	Essential Cone Vega Vega +	A, BI, C	D = 4; L = 10	–
Nokar et al.[35]	Straumann	ITI	A, BI, C (CF + PS)	BI L = 12 & DBT = 1.25 & TD = 0.35; A L = 5.5	–
Dhatrak et al.[36]	NR	NR	A, BI, S, C	D = 3.5; L = 14 D = 3.4; L = 15 D = 3.5; L = 14 D = 3.5; L = 15 D = 3.5; L = 15	Five BI analyzed
Alemayehu et al.[38]	Straumann	Standard Plus	A,BI, C	BI D = 4.1 & L = 14 & P = 0.8	Five thread designs: square, buttress, reverse buttress trapezoidal, triangular
Baggi et al.[43]	Straumann	ITI Standard (1)	A, BI	L_{tot} = 16, d = 4.10,l_{BI} = 7.5, TP = 1.15, TD = 0.24	
	Nobel Biocare	ITI Standard (2)	A, BI	L_{tot} = 17, d = 3.30, l_{BI} = 9.0, TP = 0.98, TD = 0.20	–
	Dentsply Friadent	NobelDirect	A, BI	L_{tot} = 16, d = 4.50, l_{BI} = 9.0, TP = 0.73, TD = 0.21	
		Branemark System	A, BI, S	L_{tot} = 14, d = 3.75, l_{BI} = 12, TP = 0.60, TD = 0.27	
		Ankylos	A, BI	L_{tot} = 11, d = 4.50, l_{BI} = 11, TP = 1.06, TD = 0.20	
Oswal et al.[52]	NR	NR	A, BI	D = 4; L = 12;TL = 0.5 TP = 1.2; TD = 0.42	Three thread designs: V-shaped, buttress, and reverse buttress
Aslam et al.[59]	NR	NR	A, BI, S	D = 4.5; L = 11	–

(*continued on next page*)

Table 2 (*continued*)

Reference	Manufacturer of implant	Name of implant	Implant parts	Geometric characteristics (mm)	Remarks
Wolff et al.[69]	Straumann	Straumann BL	BI	D = 4.1 & L = 10	–
		Straumann S	BI	D = 4.1 & L = 12	
		Straumann SP	BI	D = 4.1 & L = 10	
	Camlog	Camlog Plus	BI	D = 3.8, 4.3, 5 & L = 9, 11	
	Astra Tech	Astra Osseo Speed	BI	D = 4 & L = 11	
Kayabasi et al.[76]	Straumann	ITI	A, BI, C (CF+PS)	BI D = 4.1 & L = 12; A L = 4	–
de Cos Juez et al.[77]	NR	NR	BI	D = 6.8; P = 1,4,7;	–
Pirmoradian et al.[84]	NR	NR	A, BI,C	D = 4.1; L = 8.5–13	Variation of 0.6–1 mm on threads pitch
Eazhil et al.[102]	Nobel Biocare	Replace Select Tapered	A, BI	D = 3.5–5.0; L = 13–16	Different D and L analyzed
Brizuela-Velasco et al.[103]	Straumann	Straumann Standard	A, BI, C (CF+PS)	BI D = 4.8 & L = 10; A D = 4.8 & L = 5.5	–
Bachiri et al.[105]	Straumann	ITI	A, BI, C (CF+PS)	BI D = 4.1 & L = 14; A D_1 = 2.6 & D_2 = 3.6 & L = 7.2	–
Talmazov et al.[106]	Straumann	Standard Plus Tissue Level RN	A, BI	BI: D = 4.1 & L = 10 A: L = 5.5	BI: 0.2 mm TD and 1.2 mm P
Bahrami et al.[108]	NR	NR	A, BI, S, C	BI L = 11.5 & TP = 0.6	–
Cicciu et al.[110]	Megagen	AnyOne External	A, BI, S	NR	–
		AnyOne Internal	A, BI, S		
		AnyOne OneStage	A, BI, S		
Koca et al.[114]	Straumann	ITI	A, BI, C (CF+PS)	D = 4.1; L = 10	–
Ding et al.[117]	Straumann	ITI	A, BI, S, C	BI D = 4.8 and L = 10	–
de Moraes et al.[119]	Conexão Sistemas de Protese Ltda for implant Odontofix Industria e Comercio de Material Odontologico Ltda for crown	NR	A, BI, S, C	D = 3.75; L = 8.5	External hexagon implant
				D = 3.75; L = 8.5	External hexagon implant
				D = 3.75; L = 8.5	Morse taper implant
				D = 5; L = 8.5	External hexagon implant
				D = 5; L = 8.5	External hexagon implant
				D = 5; L = 8.5	Morse taper implant
Liu et al.[127]	Dentsply Implants	Ankylos	A, BI	BI D = 4 & L = 13; A D = 3.75 & L = 6	–
	Anthogyr SAS	Anthogyr	A, BI, S	BI D = 4 & L = 13; A D = 4 & L = 6	
Premnath et al.[128]	Innova	Standard threaded implant	A, BI, C	BI of threaded implant D = 4 & L = 10	–
		Standard cylindrical implant		BI od cylindrical implant D = 4.1 & L = 9	
Covani et al.[132]	Sweden Martina	Premium implant-Implant 1	A, BI, S, PS	D = 3.8; L = 13.8	Implant 1: connection A-BI made with an internal hexagon with a small collar
		Premium implant-Implant 2			Implant 2: internal hexagon connection A-BI without a collar
		Premium implant-Implant 3			Implant 3: internal connection A-BI without hexagon
		Premium implant-Implant 4			Implant 4: external hexagon connection A-BI

elements increase the computational requirements of the model due to the increase of nodes and thus of degrees of freedom. When the interest is obtaining accurate stress/strain distribution quadratic elements may be the best choice even if a large number of linear elements may allow resolving high stress gradient at lower computational costs leading to accurate results. In modeling contact or crack initiation and propagation, linear elements avoid problems seen with quadratic shape functions (e.g. convergence problems, volumetric locking).

The accuracy of FE results depends on the number of elements and nodes. It is well known that a high number of elements leads to more accurate results, but with a high computational cost. As such, to establish the mesh elements' size and thus the number of elements needed to ensure that the FE results are accurate and not affected by changing the mesh size, convergence studies are performed. In these kinds of studies, the size of the mesh elements is varied until a certain output parameter converges to a certain value. i.e. adding more elements has little effect on the output parameter but a significant effect on computational time. As such, convergence studies are fundamental to finding a good compromise between the accuracy of the solution and the computational cost.

2.3. Constitutive behavior

The mechanical behavior of a material is described through constitutive models. These models depend on a different number of parameters based on the complexity of the model. It is well known that the most simple constitutive model is isotropic linear-elastic. In this case, the constitutive behavior is represented by the following equation

$$\boldsymbol{\sigma} = \mathbb{C} : \boldsymbol{\epsilon}, \tag{1}$$

where $\boldsymbol{\sigma}$ is the second–order Cauchy stress tensor, $\mathbb{C}$ is the fourth–order elasticity tensor, characterized by minor and major symmetries and positive definite, and $\boldsymbol{\epsilon}$ is the second–order infinitesimal strain tensor. The symmetry of $\mathbb{C}$ reduces the number of independent material constants to 21. In the case of isotropic material, that is characterized by physical properties that are identical in all directions, the independent material constants of $\mathbb{C}$ are reduced to 2: Young's modulus E and Poisson's coefficient ν. While for the implant assuming an isotropic constitutive behavior is reasonable, for bone it could be not appropriate. In fact, bone is characterized by a certain degree of anisotropy, and thus assuming a more simplified constitutive model may significantly affect the FE results in terms of the stress distribution along the bone-implant interface.

In the following, the constitutive models for bone and implant with the values of the model parameters are discussed in detail.

2.3.1. Bone

The mechanical behavior of bone is complex due to its anisotropic nature and specific characteristics that are both subject and site-specific. As shown in Table 3, most FE studies adopted a simplification and have modeled cortical and trabecular bone as linearly elastic isotropic homogeneous materials. In that case, only two material constants must be used to fully define the material behavior, i.e. E and ν. Analyzing Table 3, when an isotropic homogeneous behavior is considered, the cortical bone Young's modulus ranged from 9.6 GPa to 22.8 GPa and that of cancellous bone ranged from 0.210 GPa to 1.37 GPa. Moreover, Poisson's ratio ranged from 0.18 to 0.457 in cortical bone and from 0.05 to 0.322 in trabecular bone.

To better represent the bone's mechanical behavior, some authors have considered an orthotropic material model (Table 3) that is characterized by having different properties in three perpendicular directions. Dhatrak et al. [29] performed a numerical study in which compared stress distribution around the bone-implant interface between isotropic and orthotropic material models for bone analyzing four different implants under three different loading conditions (vertical, lateral, and oblique loads). They showed an increase in von Mises stresses in orthotropic material models as compared to isotropic material models, concluding that the orthotropic model is more acceptable than the isotropic material model to predict stress along bone-implant interface. However, such a conclusion needs to be verified by combined numerical/experimental studies to validate it. The effect of considering orthotropic material properties was also investigated by Taheri et al. [87]. In their study, they used and compared two kinds of material models (i.e., isotropic and orthotropic models) for cortical and trabecular bones, concluding that by applying isotropic material model a significant part of bone stress and displacement was neglected. These neglected parts may play a crucial role in further implant design.

Another aspect to be highlighted in terms of material properties is related to the assumption of homogeneity of material distribution within the bone which may be not appropriate. It is well known that bone is characterized by a heterogeneous density field and thus heterogeneous Young's modulus distribution [86] and the heterogeneity can be modeled according to images (CT or micro-CT). In this context, Gacnik et al. [48] developed spatial and bone density-dependent isotropic and orthotropic material models of the human mandibular bone where the bone density variation has been directly determined from CT images and compared the performance of these models to the corresponding homogeneous models. They showed that the von Mises equivalent stress distribution values in the bone density-dependent orthotropic model were higher in comparison to other models and they concluded that the spatial and bone density-dependent orthotropic model may be more appropriate, as the bone's anisotropy is accounted for through the bone density. Marcian et al. [71] using micro-CT images and assuming an isotropic and linear elastic model compared different scenarios of bone material behavior (homogeneous and inhomogeneous Young's modulus distributions in bone). For the homogeneous model, they considered two different cases in which two values of E have been used, i.e. $E = 15$ GPa and $E = 5$ GPa. For the inhomogeneous case, they adopted four different models:

- Shefelbine's model

$$E = \begin{cases} 0.050 & PGI < 17000 \\ 13.636(PGI \cdot 2.21 \times 10^{-4} - 3.30) & PGI \geq 17000 \end{cases} \tag{2}$$

- Keller's model

$$E = \begin{cases} 0.050 & PGI < 17000 \\ 10.5(PGI \cdot 2.21 \times 10^{-4} - 3.30)^{2.29} & PGI \geq 17000 \end{cases} \tag{3}$$

- Snyder's model

$$E = \begin{cases} 0.050 & PGI < 17000 \\ 3.891(PGI \cdot 2.21 \times 10^{-4} - 3.30)^{2.39} & PGI \geq 17000 \end{cases} \tag{4}$$

- Inagawa's model

$$E = \begin{cases} 0.050 & PGI < 17000 \\ 17.486(PGI \cdot 2.21 \times 10^{-4} - 3.30)^{1.596} & PGI \geq 17000 \end{cases} \tag{5}$$

where E is expressed in GPa and PGI is the pixel gray intensity obtained from images. They demonstrated that the type of bone material representation significantly affects the stresses in the screw. Differences in stresses within implants might have consequences on the prediction of implant life. Hussein et al. [63] investigated the effect of different material assignments. In detail, the authors compared FE models characterized by heterogeneous E distribution with a homogeneous FE model. They showed different results between the different material assignments, highlighting a dependence of the results by implants' locations.

Table 3
Constitutive behavior and material parameters for bone (E is reported in GPa). IH: isotropic homogeneous; OH: orthotropic homogeneous; TIH: transversely isotropic homogeneous; D_1, D_2, D_3 and D_4 refer to the Lekholm & Zarb [40] classification that defines four bone types based on the relationship between cortical and trabecular bones; NP: not present; x: radial direction (direction of the cortical bone thickness); y: tangential (circumferential) direction; z: longitudinal direction. For the orthotropic model, if it is not specified, it is assumed that $\nu_{xy} = \nu_{yx}$, $\nu_{xz} = \nu_{zx}$, $\nu_{yz} = \nu_{zy}$.

Reference	Constitutive behavior	Cortical bone material parameters	Trabecular bone material parameters
Mellal et al.[15]	IH	$E = 15$, $\nu = 0.3$	$E = 1$, $\nu = 0.3$
Kitagawa et al.[18]	IH	$E = 13.7$, $\nu = 0.3$	$E = 1.37$, $\nu = 0.3$
Sevimay et al.[19]	IH	$E = 13.7$, $\nu = 0.3$	Dense $E = 1.37$, $\nu = 0.3$ Low-density $E = 1.10$, $\nu = 0.3$
Tian et al.[23]	IH	$E = 13.7$, $\nu = 0.3$	$E = 1.37$, $\nu = 0.3$
Wu et al.[25]	IH	$E = 16.7$, $\nu = 0.3$	$E = 0.759$, $\nu = 0.3$
Paracchini et al.[34]	IH	$E = 14.7$, $\nu = 0.3$	$E = 1.47$, $\nu = 0.3$
Nokar et al.[35]	IH	$E = 14.8$, $\nu = 0.3$	$E = 1.85$, $\nu = 0.3$
Baggi et al.[43]	IH	$E = 13.7$, $\nu = 0.3$	Maxillary bone $E = 0.5$, $\nu = 0.3$ Mandibular bone $E = 1$, $\nu = 0.3$
Ding et al.[45]	IH	$E = 13.7$, $\nu = 0.3$	$E = 1.37$, $\nu = 0.3$
Vairo et al.[46]	IH	$D_2E = 13.7$, $\nu = 0.3$	$D_2E = 0.5$, $\nu = 0.3$
Gacnik et al.[48]	IH	$E = 13.7$, $\nu = 0.3$	$E = 1.37$, $\nu = 0.3$
	OH	$E_x = 10.630$, $E_y = 12.510$, $E_z = 19.750$ $\nu_{xy} = 0.313$, $\nu_{yz} = 0.226$, $\nu_{xz} = 0.246$ $\nu_{yx} = 0.368$, $\nu_{zy} = 0.357$, $\nu_{zx} = 0.457$	$E_x = 0.210$, $E_y = 1.148$, $E_z = 1.148$ $\nu_{xy} = 0.055$, $\nu_{yz} = 0.322$, $\nu_{xz} = 0.055$
Oswal et al.[52]	IH	$E = 13.7$, $\nu = 0.3$	$E = 1.37$, $\nu = 0.3$
Verri et al.[53]	IH	$E = 13.7$, $\nu = 0.3$	$E = 1.37$, $\nu = 0.3$
Kim et al.[57]	IH	$E = 13$, $\nu = 0.3$	$E = 0.69$, $\nu = 0.3$
Kim et al.[58]	IH	$E = 13$, $\nu = 0.3$	$E = 0.69$, $\nu = 0.3$
Aslam et al.[59]	OH cortical bone TIH trabecular bone	$E_x = 12.6$, $E_y = 12.6$, $E_z = 19.4$ $\nu_{xy} = 0.3$, $\nu_{yz} = 0.253$, $\nu_{xz} = 0.253$ $\nu_{yx} = 0.3$, $\nu_{zy} = 0.39$, $\nu_{zx} = 0.39$	$E_x = 1.15$, $E_y = 0.2106$, $E_z = 1.15$ $\nu_{xy} = 0.055$, $\nu_{yz} = 0.01$, $\nu_{xz} = 0.322$ $\nu_{yx} = 0.01$, $\nu_{zy} = 0.055$, $\nu_{zx} = 0.322$
Lee et al.[61]	IH	$E = 13$, $\nu = 0.3$	$E = 1.3$, $\nu = 0.3$
Jafariandehkordi et al.[62]	IH	$E = 13.7$, $\nu = 0.3$	$E = 0.24$, $\nu = 0.3$
Park et al.[64]	IH	$E = 13.7$, $\nu = 0.3$	$D_3E = 1.3$, $\nu = 0.3$ $D_4E = 1.10$, $\nu = 0.3$
Linetskiy et al.[80]	IH	$D_1E = 13.7$, $\nu = 0.3$ $D_2E = 13.7$, $\nu = 0.3$ $D_3E = 13.7$, $\nu = 0.3$ $D_4E = 1.0$, $\nu = 0.3$	NP (only cortical bone) $D_2E = 1.0$, $\nu = 0.3$ $D_3E = 1.0$, $\nu = 0.3$ $D_4E = 0.2$, $\nu = 0.3$
Cinel et al.[82]	IH	$E = 13.7$, $\nu = 0.3$	$E = 1.37$, $\nu = 0.3$
Pirmoradian et al.[84]	IH	$E = 13.7$, $\nu = 0.3$	$E = 1.37$, $\nu = 0.3$
Losada et al.[85]	IH	$E = 13.4$, $\nu = 0.31$	$E = 1.37$, $\nu = 0.31$
Wang et al.[96]	OH	$E_x = 10.8$, $E_y = 13.3$, $E_z = 19.4$ $\nu_{xy} = 0.309$, $\nu_{yz} = 0.224$, $\nu_{xz} = 0.249$ $\nu_{yx} = 0.381$, $\nu_{zy} = 0.328$, $\nu_{zx} = 0.445$	$E_x = 3$, $E_y = 1$, $E_z = 0.2$ $\nu_{xy} = 0.3$, $\nu_{yz} = 0.3$, $\nu_{xz} = 0.3$
Ciucciu et al.[101]	OH	$E_x = 9.6$, $E_y = 9.6$, $E_z = 17.8$ $\nu_{xy} = 0.55$, $\nu_{yz} = 0.3$, $\nu_{xz} = 0.3$	$E_x = 0.144$, $E_y = 0.099$, $E_z = 0.344$ $\nu_{xy} = 0.23$, $\nu_{yz} = 0.11$, $\nu_{xz} = 0.13$
Brizuela-Velasco et al.[103]	IH	$D_2E = 15$, $\nu = 0.3$	$D_2E = 1$, $\nu = 0.25$
Bahrami et al.[108]	IH	$E = 14.5$, $\nu = 0.323$	$E = 1.37$, $\nu = 0.3$
Cicciu et al.[110]	OH	$E_x = 9.6$, $E_y = 9.6$, $E_z = 17.8$ $\nu_{xy} = 0.55$, $\nu_{yz} = 0.3$, $\nu_{xz} = 0.3$	$E_x = 0.144$, $E_y = 0.099$, $E_z = 0.344$ $\nu_{xy} = 0.23$, $\nu_{yz} = 0.11$, $\nu_{xz} = 0.13$
Koca et al.[114]	IH	$E = 13.4$, $\nu = 0.3$	$E = 1.37$, $\nu = 0.3$
Ding et al.[117]	OH	$E_x = 12.7$, $E_y = 17.9$, $E_z = 22.8$ $\nu_{xy} = 0.18$, $\nu_{yz} = 0.28$, $\nu_{xz} = 0.31$	$E_x = 0.511$, $E_y = 0.114$, $E_z = 0.907$ $\nu_{xy} = 0.22$, $\nu_{yz} = 0.30$, $\nu_{xz} = 0.31$
Ausiello et al.[123]	IH	$E = 13.7$, $\nu = 0.3$	$E = 0.5$, $\nu = 0.3$
Liu et al.[127]	IH	$E = 13.4$, $\nu = 0.3$	$E = 1.37$, $\nu = 0.3$
Premnath et al.[128]	IH	$E = 14.8$, $\nu = 0.3$	$D_1E = 9.5$, $\nu = 0.3$ $D_2E = 5.5$, $\nu = 0.3$ $D_3E = 1.6$, $\nu = 0.3$ $D_4E = 0.69$, $\nu = 0.3$
Ding et al.[129]	OH	$E_x = 12.7$, $E_y = 17.9$, $E_z = 22.8$ $\nu_{xy} = 0.18$, $\nu_{yz} = 0.28$, $\nu_{xz} = 0.31$	$E_x = 0.511$, $E_y = 0.114$, $E_z = 0.907$ $\nu_{xy} = 0.22$, $\nu_{yz} = 0.30$, $\nu_{xz} = 0.31$
Khened et al.[130]	IH	$E = 13.7$, $\nu = 0.26$	$E = 1.37$, $\nu = 0.31$

2.3.2. Implant

For dental implants, the constitutive behavior has been assumed to be homogeneous, isotropic, and linearly elastic. Table 4 shows the different materials used for the various components of dental implants with the values of Young's modulus E and Poisson's ratio ν. Most of the works examined the abutment screw-retained implant system. The abutment, body implant, and screw have been considered made of titanium and its alloys, with Young's modulus that ranges between 102 GPa and 136 GPa. Titanium exhibits well-documented mechanical properties and biocompatibility. However, the main issue with titanium is its gray color which can cause aesthetic problems. As such, other materials have been proposed for body implants such as zirconia [47]. The abutment is in general made of titanium or zirconia even if in some cases different materials have been used, such as in the study performed by Alemayehu et al. [38] in which the abutment is made of gold.

2.4. Bone remodeling

The bone tissue can be regarded as a self-optimizing structure that adapts to load conditions. In fact, bone is continuously subjected to remodeling processes (i.e., resorption and formation processes) during which bone changes geometric and material features to adapt to applied load [88]. As such, there is a direct control of load on bone remodeling [89]. In particular, loading is a key factor of collagen fiber orientation.

Table 4
Type of material and material parameters for dental implant assuming an isotropic and linear-elastic constitutive behavior. E: Young's Modulus (GPa); ν: Poisson's Coefficient; NP: not present; NR: not reported; CF: Crown framework; PS: Prosthetic superstructure.

Reference	Abutment material parameters	Body implant material parameters	Screw material parameters	Crown material parameters
Huang et al.[14]	Titanium E = 103, ν NR	Titanium E = 103, ν NR	NP	NP
Lin et al.[17]	Titanium E = 110, ν = 0.35	Titanium E = 110, ν = 0.35	Titanium E = 110, ν = 0.35	NP
Kitagawa et al.[18]	Titanium E = 107, ν = 0.33	Titanium E = 107, ν = 0.33	Gold alloy E = 91, ν = 0.33	NP
Sevimay et al.[19]	Titanium E = 110, ν = 0.35	Titanium E = 110, ν = 0.35	NP	Cobalt-chromium (CF) E = 218, ν = 0.33 Porcelain (PS) E = 82.8, ν = 0.35
Akca et al.[21]	Material NR E = 110, ν = 0.35	Material NR E = 110, ν = 0.35	NP	NP
Kurniawan et al.[22]	Titanium E = 110, ν = 0.35	Titanium E = 110, ν = 0.35	NP	NP
Tian et al.[23]	Titanium E = 110, ν = 0.3	Titanium E = 110, ν = 0.3	NP	NP
Chang et al.[24]	Titanium E = 102, ν = 0.3	Titanium E = 102, ν = 0.3	Titanium E = 102, ν = 0.3	Gold alloy E = 95, ν = 0.3
Wu et al.[25]	Titanium E = 104, ν = 0.3	Titanium E = 104, ν = 0.3	Titanium E = 104, ν = 0.3	NP
Ueda et al.[26]	Titanium E = 110, ν = 0.3	Titanium E = 110, ν = 0.3	NP	Gold alloy E = 100, ν = 0.3
Dhatrak et al.[29]	Titanium E = 110, ν = 0.35	Titanium E = 110, ν = 0.35	Titanium E = 110, ν = 0.35	Material NR E = 70, ν = 0.19
Badalia et al.[32]	Material NR E = 106, ν = 0.35	Material NR E = 106, ν = 0.35	NP	NP
Nokar et al.[35]	Ti-6Al-4v E = 105, ν = 0.33	Ti-6Al-4v E = 105, ν = 0.33	NP	Cr-Co alloy (CF) E = 220, ν = 0.30 Feldspathic (PS) E = 61.2, ν = 0.19
Alemayehu et al.[38]	Gold E = 136, ν = 0.37	Titanium E = 110, ν = 0.34	Titanium E = 110, ν = 0.34	Porcelain E = 68.9, ν = 0.28
Baggi et al. y	Titanium E = 114, ν = 0.34	Titanium E = 114, ν = 0.34	Titanium E = 114, ν = 0.34	NP
Fuh et al.[47]	NP	Titanium or Zirconia E = 110, ν = 0.35 for Titanium E = 210, ν = 0.31 for Zirconia	NP	Porcelain E = 70, ν = 0.19
Gacnik et al.[48]	Titanium alloy (Ti-6Al-4 V) E = 110, ν = 0.33	Titanium alloy (Ti-6Al-4 V) E = 110, ν = 0.33	NP	NP
Sarfaraz et al.[50]	Titanium alloy E = 110, ν = 0.33	Titanium alloy E = 110, ν = 0.33	Titanium E = 110, ν = 0.33	Porcelain E = 70, ν = 0.19
Oswal et al.[52]	Titanium E = 110, ν = 0.3	Titanium E = 110, ν = 0.3	NP	NP
Kim et al.[57]	Ti-grade 5 E = 114, ν = 0.33	Ti-grade 4 E = 105, ν = 0.34	Ti-grade 5 E = 114, ν = 0.33	Zirconia E = 205, ν = 0.19
Lee et al.[61]	Titanium E = 103, ν = 0.33	Titanium E = 103, ν = 0.33	Titanium E = 103, ν = 0.33	Zirconia E = 200, ν = 0.31
Park et al.[64]	Titanium E = 110, ν = 0.34	Titanium E = 110, ν = 0.34	Titanium E = 110, ν = 0.34	NR E = 140, ν = 0.28
Marcian et al.[68]	NP	Titanium E = 110, ν = 0.3	NP	NP
de Cos Juez et al.[77]	NP	Titanium E = 110, ν = 0.33	NP	NP
Linetskiy et al.[80]	Titanium E = 114, ν = 0.34	Titanium E = 114, ν = 0.34	NP	NP
Pirmoradian et al.[84]	Titanium E = 110, ν = 0.35	Titanium E = 110, ν = 0.35	NP	Porcelain E = 68.9, ν = 0.28
Losada et al.[85]	Titanium E = 110, ν = 0.32	Titanium E = 110, ν = 0.32	Titanium E = 110, ν = 0.32	Porcelain E = 68.9, ν = 0.19
Bachiri et al.[105]	Titanium E = 110, ν = 0.3	Titanium E = 110, ν = 0.3	NP	Feldsphatic porcelain FF E = 82.8, ν = 0.35
Bahrami et al.[108]	Titanium E = 110, ν = 0.31	Titanium E = 110, ν = 0.31	Titanium E = 110, ν = 0.31	Porcelain E = 82.8, ν = 0.33

Such load effect was deeply investigated by Traini et al. [91,92,154] that through histological evidence demonstrated that loaded dental implants change the bone microstructure, resulting in a predominantly transversely oriented disposition of collagen fibers. Although the mechanism with which load affects the activity of bone cells involved in remodeling processes it is still not clear, the stress and strain (or strain energy density) can usually be considered as the mechanical stimulus for bone remodeling. Frost [93] defined that remodeling, modeling, and repair determine the structural adaptation of the bone to different demands. This happens in the general context of four levels (regions) of ascending mechanical stress. The transition from one region to another is established by threshold values of microstrain. The activation of each adaptive process requires the attainment of a threshold value of microstrain, defined as minimum effective strain (MES). Fig. 3 shows

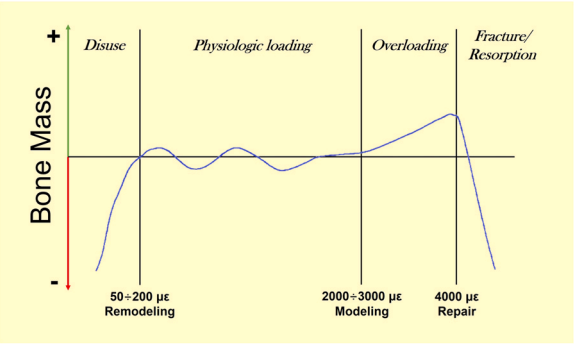

Fig. 3. Representative bone response to applied load following the Frost's theory. Region of disuse: bone exposed to low or without load has very low or zero deformation and undergoes resorption until reaching a new equilibrium between load and strain. Region of physiologic load: the bone exposed to physiologic load presents a continuous remodeling with the achievement of mass balance between resorption and apposition, with preservation of the bone mass. Region of overload: the bone exposed to a load greater than the physiologic limit presents a high deformation and gets a mass gain (corticalization) until reaching a new balance between load and deformation. Region of fracture: the bone exposed to a load greater than the limit of the overload fractures and resorbs. *y* axis: generic bone mass; *x* axis: microstrain (ϵ).

these different regions and which phenomenon occurs in each region. In particular, the bone resorbs when the strain is in the disuse region or in the resorption region, resulting in bone loss. Otherwise, when the strain is in the physiological loading or overloading region, bone formation occurs, with bone mass preservation or even increase.

Therefore, the bone remodeling response of peri-implant bone is an important aspect to be considered in the mechanical analysis of dental implants, to obtain more detailed information about the mechanical behavior of the bone-implant system and improve the long-term efficacy of dental implants. However, few studies have incorporated the remodeling processes in the FE models. In general, the remodeling process can be mathematically written as

$$\frac{d\rho}{dt} = B(M_s - M_{s_{ref}}), \tag{6}$$

where ρ represents the bone density, t is the time, B is a constant, M_s is the mechanical stimulus and $M_{s_{ref}}$ is an equilibrium point of the mechanical stimulus. If the value of M_s is less than $M_{s_{ref}}$, the quantity $\frac{d\rho}{dt}$ is negative inducing a decrease in bone density with time, meaning bone resorption. If the value of M_s is greater than $M_{s_{ref}}$, $\frac{d\rho}{dt}$ is positive and bone density increases with time, inducing bone formation.

Bone resorption is a major problem in prosthetic implants due to the fact that it causes looseness at the bone-implant interface, affecting the integrity and stability of the dental implant. While underloading is commonly regarded as a reason for bone resorption, overloading at the interface has also been suggested as a contributing factor. It is well known, that high loads cause continuum damage in the bone [94]. However, bone can repair the damage itself to some extent. However, when the loading is high, the self-repair mechanism cannot keep pace with the increasing damage, and overload resorption occurs. Thus, another aspect that numerical models need to account for to evaluate the effectiveness of dental implants over the long term, is the remodeling response at the bone-implant interface. In this context, Li et al. [94] proposed a new mathematical model for bone remodeling that accounts for potential resorption due to overloading, described by the following equation

$$\frac{d\rho}{dt} = B\left(\frac{U}{\rho} - k\right) - D\left(\frac{U}{\rho} - k\right)^2, \qquad 0 \le \rho \le \rho_{cb} \tag{7}$$

in which $\frac{d\rho}{dt}$ represents the change in density, B and D are constants, $\frac{U}{\rho}$ represents the strain energy per unit bone mass and it is the stimulus that drives the remodeling, k is the threshold value, and ρ_{cb} is the maximum density of bone. When the stimulus is small, the first linear term dominates giving a negative rate of change in ρ, i.e. underload resorption. When the stimulus is large, the second quadratic term becomes dominant, giving again a negative rate of change in ρ, i.e. overload resorption. Li et al. [94], by using this remodeling model and thus accounting for overload bone resorption, demonstrated the ability of a such model to better predict the mechanical behavior of dental implants. Chou et al. [95] implemented a remodeling algorithm to explore the effects of implant designs on bone remodeling, demonstrating that remodeling is able to predict non-homogeneous density distribution and thus elastic modulus distribution, with the implant contour that has some effect on how this is distributed. Wang et al. [96] assessed the effect of remodeling in alveolar bone before and after implantation by implementing a 3D orthotropic bone remodeling algorithm in which the strain energy density U was considered the stimulus driving the remodeling process and thus the local change of bone density (ρ). The remodeling was described by the following equations:

$$\begin{cases} \frac{d\rho}{dt} = B(\frac{U}{\rho} - (1-\delta)K_{ref}) & \text{if } \frac{U}{\rho} < (1-\delta)K_{ref} \\ \frac{d\rho}{dt} = 0 & \text{if } (1-\delta)K_{ref} < \frac{U}{\rho} < (1+\delta)K_{ref} \\ \frac{d\rho}{dt} = B(\frac{U}{\rho} - (1+\delta)K_{ref}) & \text{if } (1+\delta)K_{ref} < \frac{U}{\rho} < K_{OL} \\ \frac{d\rho}{dt} = B(K_{OL} - \frac{U}{\rho}) & \text{if } \frac{U}{\rho} > K_{OL} \end{cases} \tag{8}$$

with $\frac{U}{\rho}$ is strain energy density per unit bone mass, B is the remodeling rate constant, K_{ref} and K_{OL} are the remodeling reference values and δ is the bandwidth of the lazy zone. Starting from initial values of orthotropic Young's moduli and Poisson's ratios reported in Table 3, Wang et al. [96] calculated the change in bone density at each time step through remodeling equations (Eq. (8)). Then, based on the new density value, the orthotropic elastic moduli (E_1, E_2, and E_3 expressed in MPa) were updated according to the following equations

$$\begin{cases} E_1 = 6382 + 255(-23930 + 24000\rho) \\ E_2 = -13050 + 13000\rho \\ E_3 = -23930 + 24000\rho \end{cases} \tag{9}$$

$$\begin{cases} E_1 = 2349\rho^{2.15} \\ E_2 = 1274\rho^{2.12} \\ E_3 = 194\rho \end{cases} \tag{10}$$

where Equations (9) are related to the cortical bone ($1.2 < \rho < 2.0$, with ρ expressed in g/cm^3), whereas Equations (10) are related to the trabecular bone ($0.2 < \rho < 1.2$, with ρ expressed in g/cm^3). They showed significant differences in the stress, strain, and density distribution between the intact model and implanted model, concluding that the inclusion of remodeling is essential to obtain more insight into the mechanical response of the bone-dental implant system. Santonocito et al. [97] developed a bone remodeling algorithm able to predict the external and internal bone remodeling processes for bone tissues near the implant. The external bone remodeling has been simulated by allowing to the points on the external surface of cortical bone to change their position during simulation to account for the deposition or resorption of bone. Internal remodeling has been simulated through a change of density in trabecular and cortical bone and it has been expressed by the following law

$$\frac{d\rho}{dt} = k_r \frac{dr}{dt} S_v(\rho)\rho_t \tag{11}$$

where $\frac{dr}{dt}$ is the bone apposition/resorption rate and it is a function of tissue stress that is the stimulus that drives the remodeling, ρ_t is the fully

mineralized tissue density, k_r represents the active bone surface constant assumed equal to 0.2 and $S_v(\rho)$ is the bone surface area density, defined as the amount of bone surface area in a given bone sample divided by the bulk volume (full and empty spaces). For each time step, the model was updated considering the new bone geometry due to external remodeling, and material properties were also updated due to internal remodeling. Santonocito et al. [97] showed the ability of their remodeling algorithm to predict the implant performance over time, highlighting the importance of such an algorithm for clinicians to prevent implant failures and define an adequate implant prosthetic rehabilitation for each patient.

2.5. Bone-implant interface

Most FE studies assumed a state of 100% osseointegration at the bone-implant interface. This means that cortical and trabecular bone are perfectly bonded to the implant and neither sliding nor separation in the implant-bone interface is possible [19,21,24,26,30,34,37,43,46,48,52,55,59,63,64,67,81,82,98–101–104–107]. However, this may not occur in the clinical scenario. Thus, more complex contact and its effect on load transferring from implant to bone need to be considered in the model.

To simulate different bonding conditions at the bone-implant interface different frictional contact algorithms have been used in FE models. Tang et al. [78] defined four zones in contact: implant-bone, implant-abutment, implant-screw, and abutment-screw. They set a friction coefficient (μ) equal to 0.3 between all the titanium-titanium interfaces, 0.65 for the cortical bone-implant interface, and 0.77 for the cancellous bone-implant interface. Bahrami et al. [108] investigated the effect of surface roughness treatments on the distribution of stresses at the bone-implant interface in loaded mandibular implants. They assumed a perfect bonded condition between the implant components (body implant, abutment, screw, and crown), whereas the coronal part of the implant (in contact with cortical bone) was considered as polished ($\mu = 0.4$), and the more apical component (in contact with trabecular bone) was considered either plasma-sprayed or porous-beaded ($\mu = 1$). In their study, Wu et al. [25] considered the interface between the abutment and body implant characterized by a μ equal to 0.3, and the interfaces between body implant and cortical and trabecular bone characterized by a μ of 0.4 and 0.8, respectively. A friction coefficient μ of 0.3 has been used between bone and body implant in the study performed by Ramos et al. [109]. Kim et al. [57,58] considered perfect osseointegration for interfaces between cortical and trabecular bone, body implant and bone, and abutment and crown. At the interfaces between body implant and abutment, and abutment and screw a friction coefficient of 0.5 was used. Cicciú et al. [110] assumed perfect osseointegration at bone-implant and bone-bone interfaces and modeled the contact between the metal surfaces of the dental implant with a μ of 0.3. In the study performed by Wu et al. [33] the body implant-abutment, body implant-screw, and abutment-screw interfaces were considered in contact with a frictional coefficient of 0.3, whereas frictional coefficients of 0.65 and 0.77 were used for cortical and trabecular bone, respectively, for the interfaces between the body implant and bone. Alemayehu et al.[38] implemented a frictional contact at bone-implant interfaces with values of 0.65 between the implant and cortical bone, and 0.77 between the implant and cancellous bone. A bonded condition assumption has been considered between screw and metal framework, cortical and trabecular bone, and occlusal material and framework by Losada et al. [85], whereas a friction coefficient of 0.3 has been set between body implant and trabecular bone, body implant and cortical bone, and screw and body implant. A friction contact ($\mu = 0.3$) is defined to simulate the bone-implant interface condition in the study performed by Dhatrak et al. [36]. Cortical and trabecular bone have been modeled as bonded, whereas bone-body implant interface was modeled with $\mu = 0.2$ in [97]. Fiorillo et al. [111] modeled the bone-implant interface with a frictional contact of 0.15, whereas the contact between the cortical bone and the cancellous bone was set as bonded.

2.6. Loads and constraints

Loading and constraints adopted in the studies reported in the literature are shown in Table 5. In terms of constraints, the mesial and distal surfaces of the bone segments have been in general constrained in all degrees of freedom. In terms of loads, most FE studies considered static loads simulating not only vertical loads and horizontal forces, but also combined loads (e.g., oblique occlusal forces) to simulate more realistic conditions and thus obtain a more realistic mechanical response. However, dental implants are subjected not only to static loads but also to dynamic loads [112] that should be considered to analyze possible causes of fracture or fatigue failures of the implant. Few FE studies investigated the effect of dynamic loads. Kayabasi et al. [76] showed that dynamic load increased the stress within the implant by as much as 10–20% for dental implants with a buttress thread shape. Alemayehu et al. [38] compared the static, quasi-static and dynamic response of the implant and implanted bone under different thread designs and occlusal loading directions. They showed a remarkable increase in stress magnitude within the implant and surrounding bone in the case of dynamic loading compared to that of quasi-static and static loading conditions, concluding the need for dynamic analyses to properly understand the performance implications of a certain implant design in clinical situations. Geramizadeh et al. [113] showed that dynamic load induced greater stress in comparison with static load (about 5–10%) in the bone surrounding the implant, suggesting the necessity of transient analysis of dental implants.

2.7. FE outcomes

Most of the FE studies focused on evaluating the Von Mises stress distribution in the implant and surrounding bone [20,23,43,44,48,49,52,83,84,100,101,114–117–120]. These studies revealed that the stress field is strongly affected by some factors such as implant geometry, connection designs, implant materials, type of loading, and nature of the bone-implant interface. In terms of implant geometric characteristics, it has emerged that implant diameter, length of bone-implant interface, and thread pitch, shape, and depth are factors that play a significant role in the load transfer mechanisms and thus resultant stress distribution. It has been reported that increasing the implant diameter leads to a reduction in the crestal bone stress [45,99,119,121]. The implant diameter is more important than its length in improving the stress distribution pattern [45,102]. In their FE study, Baggi et al. [43] found that increasing the implant diameter led to a decrease in stress values and concentration areas in cortical bone, whereas more effective stress distributions for cancellous bone were experienced with increasing implant length. FE studies demonstrated that the presence of threads ensures a greater contact surface between bone and implant, and this results in a better distribution of stress in the area around the implant. Karaman et al. [122] through FE analysis investigated the effect of changing the micro-groove profile of an implant to the stress transfer to surrounding bone demonstrating that threads with a square profile are more stable than the V profile. In the FE study performed by Ausiello et al. [123], thread width and thickness resulted as dominant factors to reduce induced stresses and damage in bone. FE studies have also highlighted that the quality and quantity of bone have an impact on stress distribution and thus implant failure. The D_4 bone type characterized by a thin cortical layer and low-density trabecular bone furnishes minimal stability to the implant and limited bone-implant interface increasing the risk of failure. Anitua et al. [124] have investigated the effect of two variables (i.e., implant diameter and bone quality) on bone stress through FE analysis. They showed that regardless of the implant diameter an improvement in bone quality led to a reduction in bone stress. However, the effect of reducing bone

Table 5
Overview of static loads and constraints used in FE studies reported in the literature. FC: fully constrained; MS: mesial surface; DS: distal surface; VL: vertical load; HL: horizontal load; LL: lateral load; OL: oblique load.

Reference	Loading	Location of load	Constraints	Location of constraints
Sevimay et al.[19]	VL (total load 300 N)	150 N in buccal cusp of crown + 150 N distal fossa of crown	FC	Final element on the *x*-axis for each design
Kurniawan et al.[22]	Pressure (100 MPa)	Abutment	FC	MS and DS of bone
Chang et al.[24]	1. Axial force (100 N) 2. OL (100 N, 30° angled load)	Crown	NR	NR
Wu et al.[25]	LL (190 N, 30° with respect to implant axis)	Abutment	FC	MS and DS of bone
Ueda et al.[26]	1. VL 2. OL (15° lingually lower toward the implant axis, 60 N)	Crown	FC	MS and DS of bone
Badalia et al.[32]	1. Axial load (100 N) 2. OL (30 N)	Abutment	NR	NR
Dhatrak et al.[36]	Three loading conditions: 1. VL (100 N) (mastication force) in coronal to apical direction 2. LL of 40 N in bucco-lingual direction 3. OL (100 N) at 45° inclination with axis of implant	Crown	FC	Nodes located at bottom 1/3rd portion of bone block
Barbosa et al.[37]	1. Axial load (150 N) 2. OL (150 N, 30° angled load)	Crown	FC	Ms and DS of bone
Alemayehu et al.[38]	Combined load in the mesiodistal, buccal-lingual and apical directions	Dummy reference point located at a distance of 3 mm from the occlusal surface	FC	Interface between the implant and mandible bone
Natali et al.[41]	OL (200 N VL + 20 N HL)	Body implant	FC	MS and DS of bone
Baggi et al.[43]	OL (22°): LL along the buccal-lingual axis (100 N) + intrusive VL (250 N)	Abutment	FC	MS and DS of bone
Ding et al.[45]	Vertical and buccolingual oblique (45 degree angle, 150 N)	Abutment	FC	Nodes located at the joint surface of the condyles and the attachment regions of the masticatory muscles
Vairo et al.[46]	OL (68° angled load; VL 250 N + LL 100 N)	Abutment	FC	MS and DS of bone
Fuh et al.[47]	OL (45° to the implant axis)	Crown	FC	MS and DS of bone
Sarfaraz et al.[50]	VL(100 N) OL (45° to the longitudinal axis of the implant, 100 N)	Crown	NR	NR
Sugiura et al.[51]	Buccolingual OL (30°, 200 N)	Abutment	FC	Ms and DS of bone
Oswal et al.[52]	VL (100 N)	Abutment	FC	MS and DS of bone
Verri et al.[53]	1. Axial load (200 N) 2. OL (100 N)	1. At 4 cusp tip 2. At 2 cusp tip	FC	Anterior and posterior faces of bone block
Shirazi et al.[55]	VL (100 N)	Abutment	FC	Base supporting bone
Aslam et al.[59]	Axial load (200–800 N) OL (50–150 N, 45° to the long axis)	Abutment	FC	NR
Didier et al.[60]	VL (120 N)	Abutment	NR	NR
Lee et al.[61]	1. Occlusal VL (100 N) 2. Occlusal OL (100 N) (30° to the implants axis)	Crown	NR	NR
Jafariandehkordi et al.[62]	Pressure (1.117 MPa)	Crown	FC	MS and DS of trabecular bone
Limbert et al.[65]	Axial load (100 N)	Body implant	FC	Anterior and posterior surfaces of the μCT bone block
Marcian et al.[67]	Axial load (200 N)	Body implant	NR	NR
de Cos Juez et al.[77]	VL (150) + HL (15 N)	Body implant	NR	NR
Linetskiy et al.[80]	OL (118.2 N) 75° angled load	Abutment	FC	Nodes on the cylindrical surface of the mandible model
Pirmoradian et al.[84]	OL (45°, 180 N) Axial load (180 N)	Middle point at the center of crown	FC	MS and DS of cortical bone
Li et al.[94]	Occlusal VL (400 N)	Body implant	FC	Two cutting ends of the mandible segment
Santonocito et al.[97]	Chewing VL (100 N)	Abutment	FC	Bottom surface of the square bone system

(*continued on next page*)

Table 5 (*continued*)

Reference	Loading	Location of load	Constraints	Location of constraints
Kong et al.[99]	Axially (200 N) and buccolingually (100 N) loads	Porcelain superstructure	FC	MS and DS of bone
Cicciu et al.[101]	1. Pure traction of 400 N 2. Pure compression of 400 N 3. Flexural force of 400 N 4. Mixed tensile-bending of 400 N 5. Mixed compression bending of 400 N	Implant surface in contact with the tooth	FC	Outer side surface of the models
Eazhil et al.[102]	OL (118.2 N) 75° to the occlusal plane	Abutment	NR	NR
Brizuela et al.[103]	Load in vestibule-lingual direction (150 N), 6° with respect to implant axis	Central occlusal fossa of the crown	NR	NR
Bahrami et al.[108]	VL (200 N) + LL (20 N)	Occlusal surfaces of the crown	FC	MS and DS of cortical bone
Cicciu et al.[110]	Axial load (800)N	Abutment	FC	Lateral and bottom surfaces of bone block
Fiorillo et al.[111]	VL (400 N)	Post	FC	MS and DS of bone
Chou et al.[116]	1. VL (500 N) 2. HL (250 N)	Abutment	FC	MS and DS of bone
Schwitalla et al.[118]	1. VL (100 N) applied parallel to the implant long axis 2. OL (100 N) (30 to the implant long axis)	Crown	NR	NR
de Moraes et al.[119]	1. Axial load (200 N) OL (100 N)	1. Four points on the internal slope of the cusps 2. Two loading points in the internal slope of lingual cusps	FC	MS and DS of bone
Ausiello et al.[123]	OL (350 N) 12° angled load	Abutment	FC	Lower surface of the trabecular bone
Anitua et al.[124]	1. Axial load (200 N) 2. OL (200 N, 30° angled load)	Crown	FC	Outer faces of the bone block
Chang et al.[125]	OL (a VL of 100 N + a HL of 20 N)	Crown	FC	MS and DS of bone
Liu et al.[127]	1. VL (50 N or 100 N or 150 N) 2. HL (50 N or 100 N)	Abutment	FC	NR
Khened et al.[130]	OL (100 N) 30° angled load	Crown	FC	Nodes at the bottom of the FE bone model
Jafarian et al.[131]	VL of 200 N (along the longitudinal implant axis) + a HL of 40 N (buccolingually) at an angle of 15°	Abutment	FC	MS and DS of bone
Poovarodom et al.[133]	OL (200 N) 30° angled load	Occlusal surface with a 2-mm offset horizontally from the center to the buccal side	FC	MS and DS of bone

stresses was more pronounced by increasing the implant diameter.

FE analysis has been also used in the field of topology optimization to design new dental implants. Topology optimization aims to generate an optimized material distribution for a set of loads and constraints using FE analysis. This is performed iteratively to evaluate the performance of the new design, allowing the removal of redundant material while keeping the structural stability and functional characteristics of the implant. In this field, Chang et al. [125] applying topology optimization found that the volume of a dental implant can be reduced by 17.9% of the traditional one and the biomechanical performances were similar such as the stress of the implant, the stress of the implant-bone complex, lower displacements, and greater stiffness than the traditional implant. This volume reduction may be advantageous for bone growth due to the availability of space. Gupta et al. [126] showed that a reduction of 32–45% in the dental implant volume is possible with the implant still retaining all of its functionality.

3. The effect of load on implant stability: the microscale level as the key factor for the evolution of FE modeling and analysis

Modern dentistry cannot prescind from understanding how mechanical conditions can be controlled to optimize the speed and quality of osseointegration around oral implants. To date is known that bone has the ability to adapt its mass and structure in response to the load entity, frequency, and duration to which it is exposed [134,135]. As it was previously stated in Section 2.4 and in Fig. 3, the mechanostatic theory states that when a load is applied to the bone, the modeling and remodeling stimulus is dependent on strain magnitude, and therefore on load entity. The frequency of load can play an equally significant role. Bone mass can either be maintained by a relatively small number of loading cycles with high strains [136] or by a great number of loading cycles with low strains [137]. The entity of load determines the number of activated cells, while the level of strain is responsible for the strength of osteoblastic activity, i.e. the osteogenic effect of strains increases with increasing strain frequency [138,139]. Turner [140] formulated the following equation to explain this condition in mathematical terms:

$$\Psi = K_1 \sum_{i=1}^{n} \epsilon_i f_i \tag{12}$$

where the strain stimulus Ψ, with a proportionality constant K_1, depends on the entity of the strain (ϵ) and loading frequency f. When the frequency of load is zero ($f=0$) the strain stimulus is absent ($\Psi = 0$) [140]. The static load, therefore, does not produce any effect on the activation of bone adaptation mechanisms. Histological findings on rabbits and FE analysis by Halldin et al. [141,142] showed that the increase in bone condensation did not negatively affect the amount of primitive bone, even if the strain exceeds the ultimate and yield strain of cortical bone, indicating that static bone strains do not affect bone resorption. They also stated that the reduction in implant stability (measured in removal torque) over time can be caused by a combination of bone stress relaxation, bone resorption, and bone remodeling. After an implant is placed, the main reason for the decrease is likely to be viscoelastic bone stress relaxation. Resorption and remodeling act afterward since it takes time for a condensed bone to become revascularized. The bone modeling and remodeling start right after implant placement to heal the surgical trauma. The prestressed bone is gradually eliminated during remodeling, and the reduction in stability is explained by the remodeling of primitive bone before new bone formation increases implant stability with osseointegration.

The success of osseointegrated implants largely depends on the creation of mechanical interlocking at both the macroscale and microscale levels. The FE simulations as well as their validation with experimental results rely upon an evaluation on a macroscale level. Only in few studies [9,11,141–144], biomechanical simulations were conducted from a microscale point of view. When a dental implant is in function, the load is transmitted to the bone. Depending on bone support, bone quality, implant surface roughness, modulus of elasticity of implant material, implant diameter, and wall thickness of the implant, the load generates compressive, tensile, and shear forces at the implant-bone interface [11]. The effects of these forces need to be investigated at a microscale level, namely at the implant inter-thread level, because they can lead to a paradigm change in the systematization of factors influencing implant osseointegration. In fact, nowadays is mandatory to deepen the research at the microscale level in light of the technological development of FE software and their calculation power, along with new clinical evidence that can be used to program and validate future FE models.

Shear strength must be investigated mainly because of the fretting phenomenon. Fretting is a tribocorrosion process that occurs at the microscale level. Specifically, it is a wear process that occurs at the contact area between two materials under load and is subject to a minute relative motion by vibration or some other force [145]. According to Perona et al. [146] to define fretting, the implant mobility amplitude has to be less than 100 μm. In general, the effects of fretting on the implant-bone interface are the combination of the damage produced at the tissue level and the biological reaction. The fretting damage can be repaired by the living tissue to some extent (i.e., proper fretting), leading to cell proliferation, new formation of extracellular matrix, and new bone multicellular forming unit. However, when the fretting damage exceeds the repair ability of the living tissue, bone resorption or implant lose or other negative biological reactions would take place (i.e., improper fretting): inhibition of osteoblasts growth, increase in fibroblasts growth, activation of the immune system and bone resorption [145,147]. The critical micromovement threshold to have proper or improper fretting has been set between 50 and 150 μm. Possibly, 100 μm may be the threshold level to avoid fibrointregration and implant instability [148]. The more the shear strength, the less micromovement the implant will undergo. Hansson et al. [11] developed a mathematical model that estimates the bone-implant interfacial shear strength when a gap between the implant and bone is permitted to arise during shear situations, trying to simulate clinical conditions. A rough surface with optimized microgeometry will bring about a substantial increase in the interfacial shear strength. In the future, it will be valuable to integrate such a model into FE microscale models [143], testing the model in in-vivo conditions, to determine the real weight of fretting on the osteointegration process and to be able to predict the mechanical interlocking between the implant and supporting bone.

Regarding compressive strength and tensile strength, 2D FE studies performed by Hansson et al. [9,144] clearly have demonstrated that the implant thread geometry is a paramount element affecting the load distribution at the microscale level, and the strain on supporting bone. The peak tensile stress in the bone was located outside the top of the thread, and the peak compressive stress is placed outside the point where the lower flank of the thread passes into the curved top. It is very interesting to compare these findings with those from the histological study performed by Traini et al. [90,91,149–152,153]. They demonstrated that the thread shape is a factor influencing the amount of transverse and longitudinal bone collagen fibers [155]. A major number of transverse fibers is located under the lower flank of the thread, and longitudinal fibers arrange themselves in the interthread space, instead. The fibers' orientation changes right outside the top of the thread. In general, in the bone matrix, transversely oriented collagen fibers better resist compressive stresses, while those longitudinally oriented better resist shear stresses. In addition, from an in-vivo study, a prevalence of transversely oriented collagen fibers has been noted around immediately loaded implants and a prevalence of longitudinally oriented collagen fibers in unloaded implants [91]. This is a clear indication that loading influences the orientation of the bone collagen fibers, concurring in providing bone mechanical competence. It would be very interesting to evaluate with more sophisticated FE analysis together with in-vivo evaluation the correlation between load, bone strain, and bone collagen orientation. This is true for osseointegrated implants, but

it will be even more significant for immediately loaded or early-loaded implants. However, as previously stated by Puleo and Nanci [156], a better investigation of events at the bone-implant interface is still needed for a thorough comprehension of the bone biomechanical response. As these authors reported, morphological studies have revealed the heterogeneity of the bone-implant interface. One feature often reported, regardless of implant material, is an afibrillar interfacial zone, comparable to cement lines and laminae limitantes at natural bone interfaces. This condition should be better examined and eventually integrated into FE analysis because it can bring a change in the classical biomechanical paradigm, where implant and bone are considered "fused" together, without any interposed element. In conclusion, the opportunity to simulate and predict the bone response at the microscale level could aid the clinician in the diagnostic and follow-up phases: there might be the possibility of modulating bone response by varying the applied load, considering all other influencing factors being equal.

4. Future perspectives and conclusions

FE modeling represents an improved basis to investigate the mechanical behavior of dental implant, bone, and their interaction for the long-term stability and success of the implant. A lot of research has been performed in this direction. However, an in-depth understanding of bone-implant interaction, implant-related problems, and the development of an optimum implant design need further investigation. To do this, the following recommendations may be considered. First of all, from a geometric point of view instead of considering only a jawbone segment surrounding the implant, it may be more appropriate to model the entire jawbone for its contribution to the force exerted on the dental implant. This could be obtained from diagnostic images such as CT or Magnetic Resonance images that allow obtaining not only the patient-specific geometry but also the realistic distribution of material properties. In fact, instead of considering a homogeneous distribution of bone density and thus of E, it could be more indicated to model the bone as a heterogeneous material in terms of density and thus of E. Moreover, this may allow capturing specific conditions of bone related to the age and health condition of the patients that may have an influence on the bone-implant interaction. A pathological bone in which the bone density is significantly reduced interacts with the implant in a different way than a healthy bone, affecting the implant stability. Another recommendation is related to boundary conditions to be adopted in FE analysis. Modeling the entire jawbone may allow the incorporation of the muscle forces to account for the impact of muscles during the chewing movements that may influence the mechanical response of the bone-implant system. Modeling the muscle forces may require a detailed description of the fibers' path within the muscles. This information could be obtained by Magnetic Resonance Diffusion Tensor Imaging [157] which provides a promising approach to deriving fiber arrangements within muscle volumes. Another recommendation is related to the incorporation of bone remodeling algorithms that may allow studying the modifications in bone geometry and density over time and thus the bone-implant system mechanical behavior over time. In particular, bone remodeling algorithms should be able to simulate the micromechanical behavior of the bone-implant interface and its effects on the mechanical behavior of the bone-implant system at the macroscale level, and thus on long-term stability. To do this, a multiscale model could be useful, allowing to account for the histological arrangement of tissue constituents through multiple length scales. The incorporation of such aspect for bone could help obtain information about the relation among implant design, distribution of stress applied to the bone, and bone growth. The continuous advancement in hardware technology will aid to overcome the current computational constraints in developing such sophisticated models. Another aspect to highlight is related to dental implant design. FE analysis combined with topology optimization could help in designing implants in which the material is reduced but the implant functionality remains unaltered. The material reduction could improve bone growth due to the space availability and thus improve implant stability. Finally, in the Authors' opinion to obtain a whole understanding of the failure mechanisms of implants and the mechanical environment around the implants, strains should be investigated and a strain-based criterion should be adopted for fracture analysis. Experimental tests on bone samples have clearly indicated that bone failure has to be retained as a mainly strain-controlled event [158,159].

An important aspect to highlight is that the validation of FE modeling of dental implants is rare [8]. However, ensuring that the numerical model accurately predicts the physical phenomenon it was designed to replicate the physical quantities as strain/stress field is a crucial aspect, especially in the view to use the numerical modeling for clinical purposes [160]. Moreover, in the context of validation, sensitivity analyses should be performed due to the fact that experimental measurements may be affected by large uncertainties. As such, sensitivity studies are needed to understand the effect of uncertainty on model results As such, in the Authors' opinion future research will need clearly address the validation of numerical models of dental implants.

The ultimate aim of FE modeling and analysis is to develop an effective computational tool that could be used by the dentist in clinical practice to analyze the mechanical response of the bone-implant system and thus investigate the long-term stability to decide the more appropriate implant for the patient. In this context, machine learning-based approaches should be employed to rapidly automate FE model generation and analysis to develop a technology that could be adopted in clinical practice. For clinical application, it is necessary that the technology is fast, highly automated, and provides accurate indicators for personalized decision-making. In addition, standardization of FE modeling related to all aspects involved in the modeling is essential to the clinical applicability of FE-based models.

Funding

Funding provided by the European Union - Fondo Sociale Europeo - PON Ricerca e Innovazione 2014–2020 (azione IV.6) - FSE-REACT EU.

CRediT authorship contribution statement

Cristina Falcinelli: Conceptualization, Methodology, Writing – original draft, Writing – review & editing. **Francesco Valente**: Conceptualization, Methodology, Writing – original draft, Writing – review & editing. **Marcello Vasta**: Writing – review & editing, Funding acquisition, Supervision. **Tonino Traini**: Conceptualization, Writing – review & editing, Supervision. All authors gave final approval and agreed to be accountable for all aspects of the work.

Acknowledgments

Cristina Falcinelli and Marcello Vasta acknowledge the support of the Italian National Group for Mathematical Physics (GNFM-INdAM). Cristina Falcinelli acknowledges the funding by the European Union - Fondo Sociale Europeo - PON Ricerca e Innovazione 2014–2020 (azione IV.6) - FSE-REACT EU.

References

[1] Stein E. History of the finite element method - mathematics meets mechanics - part I: engineering developments. In: Stein E, editor. The History of Theoretical, Material and Computational Mechanics - Mathematics Meets Mechanics and Engineering. Lecture Notes in Applied Mathematics and Mechanics, 1. Springer; 2014. p. 399–442.
[2] Dolgov VY, Klyshnikov KY, Ovcharenko EA, Glushkova TV, Batranin AV, Agienko AS, et al. Finite element analysis-based approach for prediction of aneurysm-prone arterial segments. J Med Biol Eng 2019;39:102–8.
[3] Gizzi A, De Bellis ML, Vasta M, Pandolfi A. Diffusion-based degeneration of the collagen reinforcement in the pathologic human cornea. J Eng Math 2021:127.
[4] Heller MO. Chapter 32 - Finite element analysis in orthopedic biomechanics. Human Orthopaedic Biomechanics Academic Press; 2022. p. 637–58.
[5] Singh JJ, Mehta JS, Kumar R, Sapra G. FEA simulations of lower limb prosthetics.

IOP Conf Ser: Mater Sci Eng 2022;1225:012030.
[6] Lisiak-Myszke M, Marciniak D, Bieliński M, Sobczak H, Garbacewicz L, Drogoszewska B. Application of finite element analysis in oral and maxillofacial surgery-a literature review. Materials 2020;13:3063.
[7] Geng JP, Tan KBC, Liu GR. Application of finite element analysis in implant dentistry: a review of the literature. J Prosthet Dent 2001;85:585–98.
[8] Chang Y, Tambe AA, Maeda Y, Wada M, Gonda T. Finite element analysis of dental implants with validation: to what extent can we expect the model to predict biological phenomena? A literature review and proposal for classification of a validation process. Int J Implant Dent 2018;4:7.
[9] Hansson S, Werke M. The implant thread as a retention element in cortical bone: the effect of thread size and thread profile: a finite element study. J Biomech 2003;36:1247–58.
[10] Hansson S, Norton M. The relation between surface roughness and interfacial shear strength for bone-anchored implants. A mathematical model. J Biomech 1999;32:829–36.
[11] Hansson S, Loberg J, Mattisson I, Ahlberg E. Global biomechanical model for dental implants. J Biomech 2011;44:1059–65.
[12] Van Oosterwyck H, Duyck J, VanderSloten J, Van der Perre G, De Cooman M, Lievens S, et al. The influence of bone mechanical properties and implant fixation upon bone loading around oral implants. J Biomech 1998;9:407–18.
[13] Chun HJ, Cheong SY, Han JH, Heo SJ, Chung JP, Rhyu IC, et al. Evaluation of design parameters of osseointegrated dental implants using finite element analysis. J Oral Rehabil 2002;29:565–74.
[14] Huang HM, Lee SY, Yeh CY, Lin CT. Resonance frequency assessment of dental implant stability with various bone qualities: a numerical approach. Clin Oral Impl Res 2002;13:65–74.
[15] Mellal A, Wiskott HWA, Botsis J, Scherrer SS, Belser UC. Stimulating effect of implant loading on surrounding bone. Comparison of three numerical models and validation by in vivo data. Clin Oral Impl Res 2004;15:239–48.
[16] Zhiyong L, Arataki T, Shimamura I, Kishi M. The influence of prosthesis designs and loading conditions on the stress distribution of tooth-implant supported prosthesis. Bull Tokyo Dent Coll 2004;45:213–21.
[17] Lin CL, Kuo YC, Lin TS. Effects of dental implant length and bone quality on biomechanical responses in bone around implants: a 3-D non-linear finite element analysis. Biomed Eng - Appl Basis Commun 2005;17:44–9.
[18] Kitagawa T, Tanimoto Y, Nemoto K, Aida M. Influence of cortical bone quality on stress distribution in bone around dental implant. Dent Mater J 2005;24:219–24.
[19] Sevimay M, Turhan F, Kiliçarslan MA, Eskitascioglu G. Three-dimensional finite element analysis of the effect of different bone quality on stress distribution in an implant-supported crown. J Prosthet Dent 2005;93:227–34.
[20] Heckmann SM, Karl M, Wichmann MG, Graef F, Taylor TD. Loading of bone surrounding implants through three-unit fixed partial denture fixation: a finite-element analysis based on in vitro and in vivo strainmeasurements. Clin Oral Impl Res 2006;17:345–50.
[21] Akca K, Cehreli MC. Biomechanical consequences of progressive marginal bone loss around oral implants: a finite element stress analysis. Med Bio Eng Comput 2006;44:527–35.
[22] Kurniawan D, Nor FM, Lim JY. Finite element analysis of bone-implant biomechanics: refinement through featuring various osseointegration conditions. Int J Oral Maxillofac Surg 2012;41:1090–6.
[23] Tian K, Chen J, Han L, Yang J, Huang W, Wu D. Angled abutments result in increased or decreased stress on surrounding bone ofsingle-unit dental implants: a finite element analysis. Med Eng Phys 2012;34:1526–31.
[24] Chang HS, Chen YC, Hsieh YD, Hsu ML. Stress distribution of two commercial dental implant systems: a three-dimensional finite element analysis. J Dent Sci 2013;8:261–71.
[25] Wu AYJ, Hsu JT, Chee W, Lin YT, Fuh LJ, Huang HL. Biomechanical evaluation of one-piece and two-piece small-diameter dental implants: in-vitro experimental and three-dimensional finite element analyses. J Formos Med Assoc 2016;115:794–800.
[26] Ueda N, Takayama Y, Yokoyama A. Minimization of dental implant diameter and length according to bone quality determined by finite element analysis and optimized calculation. J Prosthodont Res 2017;61:324–32.
[27] Poovarodom P, Sae-Lee D, Suriyawanakul J. The 3D finite element analysis of stress distribution in implant supported single crown with different abutment designs. Eng Appl Sci Res 2018;45:240–50.
[28] Ozturk O, Kulunk T, Kulunk S. Influence of different implant-abutment connections on stress distribution in singletilted implants and peripheral bone: a three-dimensional finite element analysis. Biomed Mater Eng 2018;29:513–26.
[29] Dhatrak P, Girme V, Shirsat U, Sumanth S, Deshmukh V. Significance of orthotropic material models to predict stress around bone-implant interface using numerical simulation. BioNanoSci 2019;9:652–9.
[30] Shash M, Nazha H, Abbas W. Influence of different abutment designs on the biomechanical behavior of one-piece zirconia dental implants and their surrounding bone: a 3D-FEA. IRBM 2019;40:313–9.
[31] Oliveira H, BrizuelaVelasco A, Ríos-Santo JV, Lasheras FS, Lemos BF, Gil FJ, et al. Effect of different implant dsigns on strain and stress distribution under non-axial loading: a three-dimensional finite element analysis. Int J Environ Res Public Health 2020;17:4738.
[32] Badalia I, Kumar M, Bansal A, Batra R. Evaluation of stress patterns in bone around implants for different abutment angulations under axial and oblique loading in anterior maxillary region—a finite element analysis. Dent J Adv Stud 2020;8:60–4.
[33] Wu YL, Tsai MH, Chen HS, Chang YT, Lin TT, Wu AYJ. Biomechanical effects of original equipment manufacturer and aftermarket abutment screws in zirconia abutment on dental implant assembly. Sci Rep 2020;10:18406.
[34] Paracchini L, Barbieri C, Redaelli M, DiCroce D, Vincenzi C, Guarnieri R. Finite element analysis of a new dental implant design optimized for the desirable stress distribution in the surrounding bone region. Prostesis 2020;2:225–36.
[35] Nokar S, Jalali H, Nozari F, Arshad M. Finite element analysis of stress in bone and abutment-implant interface under static and cyclic loadings. Front Dent 2020;17:1–8.
[36] Dhatrak P, Shirsat U, Sumanth S, Deshmukh V. Numerical investigation on stress intensity around bone-implant interface by 3-dimensional FEA and experimental verification by opticaltechnique. Mater Today: Proc 2021;39:35–41.
[37] Barbosa FT, Zanatta LCS, de SouzaRendohl E, Gehrke SA. Comparative analysis of stress distribution in one-piece and two-piece implants with narrow and extra-narrow diameters: a finite element study. PLoS One 2021;16:e0245800.
[38] Alemayehu DB, Jeng YR. Three-Dimensional Finite Element Investigation into effects of implant thread design and loading rate on stress distribution in dental implants and anisotropic bone. Materials 2021;14:6974.
[39] Milone D, Fiorillo L, Alberti F, Cervino G, Filardi V, Pistone A, et al. Stress distribution and failure analysis comparison between zirconia and titanium dental implants. Procedia Struct Integr 2022;41:680–91.
[40] Oliveira MR, Gonçalves A, Gabrielli MAC, de Andrade CR, Vieira EH, Pereira-Filho VA. Evaluation of alveolar bone quality: correlation between histomorphometric analysis and Lekholm and Zarb classification. J Craniofac Surg 2021;32:2114–8.
[41] Natali AN, Pavan PG, Ruggero AL. Analysis of bone-implant interaction phenomena by using a numerical approach. Clin Oral Impl Res 2006;17:67–74.
[42] Yang J, Xiang HJ. A three-dimensional finite element study on the biomechanical behavior of an FGBM dental implant in surrounding bone. J Biomech 2007;40:2377–85.
[43] Baggi L, Cappelloni I, DiGirolamo M, Maceri F, Vairo G. The influence of implant diameter and length on stress distribution of osseointegrated implants related to crestal bone geometry: a three dimensional finite element analysis. J Prosthet Dent 2008;100:422–31.
[44] Baggi L, Cappelloni I, Maceri F, Vairo G. Stress-based performance evaluation of osseointegrated dental implantsby finite-element simulation. Simul Model Pr Theory 2008;16:971–87.
[45] Ding X, Liao SH, Zhu XH, Zhang XH, Zhang L. Effect of diameter and length on stress distribution of the alveolar crest aroundimmediate loading implants. Clin Implant Dent Relat Res 2009;11:279–87.
[46] Vairo G, Saonnino G. Comparative evaluation of osseointegrated dental implants based on platform-switching concept: influence of diameter, length, thread shape, and in-bone positioning depth onstress-based performance. Comput Math Methods Med 2013;2013:250929.
[47] Fuh LJ, Hsu JT, Huang HL, Chen MY, Shen YW. Biomechanical investigation of thread designs and interface conditions of zirconia and titanium dental implants with bone: three dimensional numeric analysis. Int J Oral Maxillofac Implants 2013;28:e64–71.
[48] Gacnik F, Ren Z, Hren NI. Modified bone density-dependent orthotropic material modelof human mandibular bone. Med Eng Phys 2014;36:1684–92.
[49] Rezende CE, Chase-Diaz M, Costa MD, Albarracin ML, Paschoeto G, Sousa EA, et al. Stress distribution in single dental implant system: three-dimensional finite element analysis based on an in vitro experimental model. J Craniofac Surg 2015;26:2196–200.
[50] Sarfaraz H, Paulose A, Shenoy KK, Hussain A. A three-dimensional finite element analysis of a passive andfriction fit implant abutment interface and the influence of occlusal table dimension on the stress distribution patternon the implant and surrounding bone. J Indian Prosthodont Soc 2015;15:229–36.
[51] Sugiura T, Yamamoto K, Horita S, Murakami K, Tsutsumi S, Kirita T. The effects of bone density and crestal cortical bone thickness onmicromotion and peri-implant bone strain distribution in an immediately loaded implant: a nonlinear finite element analysis. J Periodontal Implant Sci 2016;46:152–65.
[52] Oswal MM, Amasi UN, Oswal MS, Bhagat AS. Influence of three different implant thread designs on stress distribution: a three-dimensional finite element analysis. J Indian Prosthodont Soc 2016;16:359–65.
[53] Verri FR, Cruz RS, de Souza Batista VE, Almeida DA, Verri AC, Lemos CA, et al. Can the modeling for simplification of a dental implant surface affect the accuracy of 3D finite element analysis? Comput Methods Biomech Biomed Eng. 2016;19:1665–72.
[54] Zhang G, Yuan H, Chen X, Wang W, Chen J, Liang J, et al. A three-Dimensional finite element study onthe biomechanical simulation of various structured dental implants and their surrounding bone tissues. Int J Dent 2016;2016:4867402.
[55] Shirazi HA, Ayatollahi M, Karimi A, Navidbakhsh M. A comparative finite element analysis of two types of axial and radial functionally graded dental implants with titanium one around implant-bone interface. Sci Eng Compos Mater 2017;24:747–54.
[56] Minatel L, Verri FR, Kudo GAH, de Faria Almeida DA, de Souza Batista VE, Lemos CAA, et al. Effect of different types of prosthetic platforms on stress-distribution indental implant-supported prostheses. Mater Sci Eng C Mater Biol Appl 2017;71:35–42.
[57] Kim WH, Song ES, Ju KW, Lee JH, Kim MY, Lim D, et al. Finite element analysis of novel separable fixture for easy retrievement in case with peri-implantitis. Materials 2019;12:235.
[58] Kim WH, Lee JC, Lim D, Heo YK, Song ES, Lim YJ, et al. Optimized dental implant fixture design for the desirable stress distribution in the surrounding bone region: a biomechanical analysis. Materials 2019;12:2749.
[59] Aslam A, Hassan SH, Aslam HM, Khan DA. Effect of platform switching on peri-implant bone: a 3D finite element analysis. J Prosdent 2019;6:935–40.

[60] Didier P, Piotrowski B, LeCoz G, Joseph D, Bravetti P, Laheurte P. Finite element analysis of the stress field in peri-implant bone: a parametric study of influencing parameters and their interactions for multi-objective optimization. Appl Sci 2020;10:5973.
[61] Lee JH, Jang HY, Lee SY. Finite element analysis of dental implants with zirconia crown restorations: conventional cement-retained vs. cementless screw-retained. Materials 2021;14:2666.
[62] Jafariandehkordi A, Jafariandehkordi Z. A finite element optimization of the design variables of a dental implant screw based on the mechanostat theory. Comput Methods Prog Biomed Update 2021;1:100033.
[63] Hussein MO, Alruthea MS. Evaluation of bone-implant interface stress and strain using heterogeneous mandibular bone properties based on different empirical correlations. Eur J Dent 2021;15:454–62.
[64] Park J, Park S, Kang I, Noh G. Biomechanical effects of bone quality and design features in dental implants in long-term bone stability. J Comput Des Eng 2022;9:1538–48.
[65] Limbert G, van Lierde C, Muraru OL, Walboomers XF, Frank M, Hansson S, et al. Trabecular bone strains around a dental implant and associated micromotions—a micro-CT-based three-dimensional finite element study. J Biomech 2010;43:1251–61.
[66] Wirth AJ, Muller R, van Lenthe GH. The discrete nature of trabecular bone microarchitecture affects implant stability. J Biomech 2012;45:1060–7.
[67] Marcian P, Borak L, Valasek J, Kaiser J, Florian Z, Wolff J. Finite element analysis of dental implant loading on atrophicand non-atrophic cancellous and cortical mandibular bone - a feasibility study. J Biomech 2014;47:3830–6.
[68] Marcian P, Wolff J, Horackova L, Kaiser J, Zikmund T, Borak L. Micro finite element analysis of dental implants under different loading conditions. Comput Biol Med 2018;96:157–65.
[69] Wolff J, Narra N, Antalainen AK, Valasek J, Kaiser J, Sandor GK, et al. Finite element analysis of bone loss around failing implants. Mater Des 2014;61:177–84.
[70] Liao SH, Zhu XH, Xie J, Sohodeb VK, Ding X. Influence of trabecular bone on peri-implant stress and strain based on micro-CT finite element modeling of beagle dog. Biomed Res Int 2016;2016:3926941.
[71] Marcian P, Borak L, Zikmund T, Horackova L, Kaiser J, Joukal M, et al. On the limits of finite element models created from (micro)CT datasets and used in studies of bone-implant-related biomechanical problems. J Mech Behav Biomed Mater 2021;117:104393.
[72] Pakdel A, Robert N, Fialkov J, Maloul A, Whyne C. Generalized method for computation of true thickness and X-ray intensity information in highly blurred submillimeter bone features in clinical CT images. Phys Med Biol 2012;57:8099–116.
[73] Falcinelli C, Schileo E, Pakdel A, Whyne C, Cristofolini L, Taddei F. Can CT image deblurring improve finite element predictions at the proximal femur? J MechBehav Biomed Mater 2016;63:337–51.
[74] Nimbalkar S, Dhatrak P, Gherde C, Joshi S. A review article on factors affecting bone loss in dental implants. Mater Today: Proc 2021;43:970–6.
[75] Perriard J, Wiskott WA, Mellal A, Scherrer SS, Botsis J, Belser UC. Fatigue resistance of ITI implant-abutment connectors - a comparison of the standard cone with a novel internally keyed design. Clin Oral Implants Res 2002;13:542–9.
[76] Kayabasi O, Yuzbasıoglu E, Erzincanli F. Static, dynamic and fatigue behaviors of dental implant using finite element method. Adv Eng Softw 2006;37:649–58.
[77] de Cos Juez FJ, SanchezLasheras F, Garcia Nieto PJ, Álvarez-Arenal A. Non-linear numerical analysis of a double-threaded titanium alloy dental implant by FEM. Appl Math Comput 2008;206:952–67.
[78] Tang CB, Liul SY, Zhou GX, Yu JH, Zhang GD, Bao YD, et al. Nonlinear finite element analysis of three implant-abutment interface designs. Int J Oral Sci 2012;4:101–8.
[79] Ayllon JM, Navarro C, Vázquez J, Domínguez J. Fatigue life estimation in dental implants. Eng Fract Mech 2014;123:34–43.
[80] Linetskiy I, Demenko V, Linetska L, Yefremov O. Impact of annual bone loss and different bone quality on dental implant success - a finite element study. Comput Biol Med 2017;91:318–25.
[81] Cervino G, Romeo U, Lauritano F, Bramanti E, Fiorillo L, D'Amico C, et al. Fem and von mises analysis of OSSTEM dental implant structural components: evaluation of different direction dynamic loads. Open Dent J 2018;12:219–29.
[82] Cinel S, Celik E, Sagirkaya E, Sahin O. Experimental evaluation of stress distribution with narrow diameter implants: a finite element analysis. J Prosthet Dent 2018;119:417–25.
[83] Bayata F, Yildiz C. The effects of design parameters on mechanical failure of Ti-6Al-4V implants using finite element analysis. Eng Fail Anal 2020;110:104445.
[84] Pirmoradian M, Naeeni HA, Firouzbakht M, Toghraie D, Khabaz MK, Darabi R. Finite element analysis and experimental evaluation on stress distribution and sensitivity of dental implants to assess optimum length and thread pitch. Comput Methods Prog Biomed 2020;187:105258.
[85] Losada HF, Goncalves E, Valin JL, Ide L. Analysis of the influence of parafunctional loads on the bone-prosthesis system: a non-linear finite element analysis. J Biomed Sci Eng 2021;14:223–32.
[86] Falcinelli C, Whyne C. Image-based finite-element modeling of the human femur. Comput Methods Biomech Biomed Eng 2020;14:1138–61.
[87] Taheri RA, Jarrahi A, Farnoosh G, Karimi A. A comparative finite element simulation of stress in dental implant-bone interface using isotropic and orthotropic material models in three mastication cycles. J Braz Soc Mech Sci Eng 2018;40:489.
[88] Haiat G, Wang HL, Brunski J. Effects of biomechanical properties of the bone-implant interface on dental implant stability: from in silico approaches to the patient's mouth. Annu Rev Biomed Eng 2014;16:187–213.
[89] Wolff J. The law of bone remodeling. Das Gesetz der Transformation der Knochen. Berlin: A. Hirchwild; 1892.
[90] Traini T, Degidi M, Caputi S, Strocchi R, DiIorio D, Piattelli A. Collagen fiber orientation in human peri-implant bone around immediately loaded and unloaded titanium dental implants. J Periodo 2005;76:83–9.
[91] Traini T, Degidi M, Strocchi R, Caputi S, Piattelli A. Collagen fiber orientation near dental implants in human bone:do their organization reflect differences in loading? J Biomed Mater Res B Appl Biomater 2005;74:538–46.
[92] Traini T, Pecora G, Iezzi G, Piattelli A. Preferred collagen fiber orientation human peri-implant bone after a short- and long-term loading period: a case report. J Oral Implant 2006;32:177–81.
[93] Frost HM. Bone mass and the mechanostat: a proposal. Anat Rec 1987;219:1–9.
[94] Li J, Li H, Shi L, Fok AS, Ucer C, Devlin H, et al. A mathematical model for simulating the bone remodeling process under mechanical stimulus. Dent Mater 2007;23:1073–8.
[95] Chou HY, Jagodnik JJ, Muftu S. Predictions of bone remodeling around dental implant systems. J Biomech 2008;41:1365–73.
[96] Wang C, Fu G, Deng F. Difference of natural teeth and implant-supported restoration: a comparison of bone remodeling simulations. J Dent Sci 2015;10:190–200.
[97] Santonocito D, Nicita F, Risitano GA. A Parametric study on a dental implant geometry influence on bone remodelling through a Numerical algorithm. Prosthesis 2021;3:157–72.
[98] Gallas MM, Abeleira MT, Fernández JR, Burguera M. Three-dimensional numerical simulation of dental implants as orthodontic anchorage. Eur J Orthod 2005;27:12–6.
[99] Kong L, Sun Y, Hu K, Li D, Hou R, Yang J, et al. Bivariate evaluation of cylinder implant diameter and length: a three-dimensional finite element analysis. J Prosthodont 2008;17:286–93.
[100] Ibrahim MM, Thulasingam C, Nasser KSGA, Balaji V, Rajakumar M, Rupkumar P. Evaluation of design parameters of dental implant shape, diameter and length on stress distribution: a finite element analysis. J Indian Prosthodont Soc 2011;11:165–71.
[101] Cicciú M, Cervino G, Bramanti E, Lauritano F, Lo Gudice G, Scappaticci L, et al. FEM analysis of mandibular prosthetic overdenture supported by dental implants: evaluation of different retention methods. Comput Math Methods Med 2015;943839:943839.
[102] Eazhil R, Swaminathan SV, Gunaseelan M, Kannan GV, Alagesan C. Impact of implant diameter and length onstress distribution in osseointegrated implants:a 3D FEA study. J Int Soc Prev Community Dent 2016;6:590–6.
[103] Brizuela-Velasco A, Pérez-Pevida E, Jiménez-Garrudo A, Gil-Mur FJ, Manero JM, Punset-Fuste M, et al. Mechanical characterisation and biomechanical and biological behaviours of Ti-Zr binary-alloy dental implants. BioMe Res Int 2017;2017:2785863.
[104] Geramizadeh M, Katoozian H, Amid R, Kadkhodazadeh M. Three-dimensional optimization and sensitivity analysis of dental implant thread parameters using finite element analysis. J Korean Assoc Oral Maxillofac Surg 2018;44:59.
[105] Bachiri A, Djebbar N, Boutabout B, Serier B. Effect of different impactor designs on biomechanical behavior in the interface bone-implant: a comparative biomechanics study. Comput Methods Prog Biomed 2020;197:105723.
[106] Talmazov G, Veilleux N, Abdulmajeed A, Bencharit S. Finite element analysis of a one-piece zirconia implant in anterior single tooth implant applications. PLoS One 2020;15:e0229360.
[107] Taharou B, Merdji A, Hillstrom R, Benaissa A, Roy S, Della N, et al. Biomechanical evaluation of bone quality effect on stresses atbone-implant interface: a finite element study. J Appl Comput Mech 2020;7:1266–75.
[108] Bahrami B, Shahrbaf S, Mirzakouchaki B, Ghalichi F, Ashtiani M, Martin N. Effect of surface treatment on stress distribution in immediately loaded dental implants–a 3D finite element analysis. Dent Mater J 2014;30:e89–97.
[109] Ramos A, Mesnard M. Finite element model to predict bone loss arounddental implant. Comput Methods Biomech Biomed Eng. 2019;22:548–50.
[110] Cicciú M, Cervino G, Terranova A, Risitano G, Raffaele M, Cucinotta F, et al. Prosthetic and mechanical parameters of the facialbone under the load of different dental implant shapes: a parametric study. Prosthesis 2019;1:41–53.
[111] Fiorillo L, Milone D, D'Andrea D, Santonocito D, Risitano G, Cervino G, et al. Finite element analysis of zirconia dental implant. Prosthesis 2022;4:490–9.
[112] Khosravani MR. Mechanical behavior of restorative dental composites under various loading conditions. J Mech Behav Biomed Mater 2019;93:151–7.
[113] Geramizadeh M, Katoozian H, Amid R, Kadkhodazadeh M. Finite element analysis of dental implants with and without microthreads under static and dynamic loading. J Long-Term Eff Med Implants 2017;27:22–35.
[114] Koca OL, Eskitascioglu G, Usumez A. Three-dimensional finite-element analysis of functional stresses in different bone locations produced by implants placed in the maxillary posterior region of the sinus floor. J Prosthet Dent 2005;93:38–44.
[115] Tiossi R, Vasco MA, Lin L, Conrad HJ, Bezzon OL, Ribeiro RF, et al. Validation of finite element models for strain analysis of implant-supported prostheses using digital image correlation. Dent Mater J 2013;29:788–96.
[116] Chou IC, Lee SY, Jiang CP. Effects of implant neck design on primary stability and overload in a type IV mandibular bone. Int J Numer Method Biomed Eng 2014;30:1223–37.
[117] Ding X, Liao SH, Zhu XH, Wang HM. Influence of orthotropy on biomechanics of peri-implant bone in complete mandible model with full dentition. Biomed Res Int 2014;2014.
[118] Schwitalla AD, Abou-Emara M, Spintig T, Lackmann J, Müller WD. Finite element analysis of the biomechanical effects of PEEK dental implants on the peri-implant bone. J Biomech 2015;48:1–7.
[119] Moraes SLDD, Verri FR, Santiago Júnior JF, Almeida DADF, Lemos CAA, Gomes JMDL, et al. Three-dimensional finite element analysis of varying diameter and

connection type in implants with high crown-implant ratio. Braz Dent J 2018;29:36–42.
[120] Castilla R, Forero L, González-Estrada OA. Comparative study of the influence of dental implant design on the stress and strain distribution using the finite element method. J Phys Conf Ser 2019;1159:012016.
[121] Himmlova L, Kacovsky A, Konviickova S. Influence of implant length and diameter on stress distribution: a finite element analysis. J Prosthet Dent 2004;91:20–5.
[122] Karaman H, Yuce C, Karpat F, Dhanasekaran L, Khandaker M. Structural analysis of dental implants with various micro grove profiles. IRJAES 2018;3:101–4.
[123] Ausiello P, Franciosa P, Martorelli M, Watts DC. Effects of thread features in osseointegrated titanium implants using a statistics-based finite element method. Dent Mater J 2012;28:919–27.
[124] Anitua E, Larrazabal Saez de Ibarra N, MoralesMartín I, Saracho Rotaeche L. Influence of dental implant diameter and bone quality on the biomechanics of single-crown restoration. A finite element analysis. Dent J 2021;9:103.
[125] Chang CL, Chen CS, Huang CH, Hsu ML. Finite element analysis of the dental implant using a topology optimization method. Med Eng Phys 2012;34:999–1008.
[126] Gupta Y, Iyer R, Dommeti VK, Nutu E, Rana M, Merdji A, et al. Design of dental implant using design of experiment and topology optimization: a finite element analysis study. Proc Inst Mech Eng H: J Eng Med 2021;235:157–66.
[127] Liu S, Tang C, Yu J, Dai W, Bao Y, Hu D. The effect of platform switching on stress distribution in implants and periimplant bone studied by nonlinear finite element analysis. J Prosthet Dent 2014;112:1111–8.
[128] Premnath K, Sridevi J, Kalavathy N, Nagaranjani P, Sharmila MR. Evaluation of stress distribution in bone of different densities using different implant designs: a three-dimensional finite element analysis. J Indian Prosthodont Soc 2013;13:555–9.
[129] Ding X, Liao SH, Zhu XH, Wang HM, Zou BJ. Effect of orthotropic material on finite element modeling of completely dentate mandible. Mater Des 2015;84:144–53.
[130] Khened V, Bhandarkar S, Dhatrak P. Dental implant thread profile optimization using Taguchi approach. Mater Today Proc 2022.
[131] Jafarian M, Mirhashemi FS, Emadi N. Finite element analysis of stress distribution around a dental implant with different amounts of bone loss: an in vitro study. Dent Med Probl 2019;56:27–32.
[132] Covani U, Ricci M, Tonelli P, Barone A. An evaluation of new designs in implant-abutment connections: a finite element method assessment. Implant Dent 2013;22:263–7.
[133] Poovarodom P, Rungsiyakull C, Suriyawanakul J, Li Q, Sasaki K, Yoda N, et al. Effect of implant placement depth on bone remodeling on implant-supported single zirconia abutment crown: a 3D finite element study. J Prosthodont Res 2022.
[134] Mosley JR, Lanyon LE. Strain rate as a controlling influence on adaptive modeling in response to dynamic loading of the ulna in growing male rats. Bone 1998;23:313–8.
[135] Qin YX, Rubin CT, McLeod KJ. Nonlinear dependence of loading intensity and cycle number in the maintenance of bone mass and morphology. J Orthop Res 1998;16:482–9.
[136] Rubin CT, Lanyon LE. Regulation of bone formation by applied dynamic loads. J Bone Jt Surg Am 1984;66:397–402.
[137] Lanyon LE, Hampson WG, Goodship AE, Shah JS. Bone deformation recorded in vivo from strain gauges attached to the human tibial shaft. Acta Orthop Scand 1975;46:256–68.
[138] Forwood MR, Turner CH. Skeletal adaptations to mechanical usage: results from tibial loading studies in rats. Bone 1995;17:197S–205S.
[139] Frost HM. Bone remodeling and its relationship to metabolic bone disease. Charles C Thomas Springfield; 1973. (III).
[140] Turner CH. Three rules for bone adaptation to mechanical stimuli. Bone 1998;23:399–407.
[141] Halldin A, Jimbo R, Johansson CB, Wennerberg A, Jacobsson M, Albrektsson T, et al. The effect of static bone strain on implant stability and bone remodeling. Bone 2011;49:783–9.
[142] Halldin A, Jimbo R, Johansson CB, Wennerberg A, Jacobsson M, Albrektsson T, et al. Implant stability and bone remodeling after 3 and 13 days of implantation with an initial static strain: initial implant stability. Clin Oral Implants Res 2014;16:383–93.
[143] Halldin A, Ander M, Jacobsson M, Hansson S. Simulation of the mechanical interlocking capacity of a rough bone implant surface during healing. BioMed Eng OnLine 2015;14:45.
[144] Hansson S. A conical implant-abutment interface at the level of the marginal bone improves the distribution of stresses in the supporting bone: an axisymmetric finite element analysis. Clin Oral Implants Res 2003;14:286–93.
[145] Gao SS, Zhang YR, Zhu ZL, Yu HY. Micromotions and combined damages at the dental implant/bone interface. Int J Oral Sci 2012;4:182–8.
[146] Perona PG, Lawrence J, Paprosky WG, Patwardhan AG, Sartori M. Acetabular micromotion as a measure of initial implant stability in primary hip arthroplasty. An in vitro comparison of different methods of initial acetabular component fixation. J Arthroplast 1992;7:537–47.
[147] Noumbissi S, Scarano A, Gupta S. A Literature review study on atomic ions dissolution of titanium and its alloys in implant dentistry. Materials 2019;12:368.
[148] Brunski JB. Avoid pitfalls of overloading and micromotion of intraosseous implants. Dent Implant Update 1993;4:77–81.
[149] Traini T, Degidi M, Murmura G, Piattelli A, Caputi S. Bone microstructure evaluation near unloaded dental implants combining confocal scanning laser microscopy, circularly polarized light microscopy, and SEM backscattered electrons imaging. Int J Immunopathol Pharm 2007;20:37–41.
[150] Traini T, Novaes AB, Papalexiou V, Piattelli A. Influence of interimplant distance on bone microstructure: a histomorphometric study in dogs. Clin Implant Dent Relat Res 2008;10:1–10.
[151] Traini T, Pecora G, Iezzi G, Piattelli A. Preferred collagen fiber orientation human peri-implant bone after a short- and long-term loading period: a case report. J Oral Implant 2006;32:177–81.
[152] Traini T, De Paoli S, Caputi S, Iezzi G, Piattelli A. Collagen fiber orientation near a fractured dental implant after a 5-year loading period: case report. Implant Dent 2006;15:70–6.
[153] Traini T, Neugebauer J, Thams U, Zöller JE, Caputi S, Piattelli A. Peri-implant bone organization under immediate loading conditions: collagen fiber orientation and mineral density analyses in the minipig model. Clin Oral Implants Res 2009;11:41–51.
[154] Traini T, Degidi M, Strocchi R, Caputi S, Piattelli A. Collagen fiber orientation near dental implants in human bone: do their organization reflect differences in loading? J Biomed Mater Res B Appl Biomater 2005;74:538–46.
[155] Valente F, Scarano A, Murmura G, Varvara G, Sinjari B, Mandelli F, et al. Collagen fibres orientation in the bone matrix around dental implants: does the implant's thread design play a role? Int J Mol Sci 2021;22:7860.
[156] Puleo DA, Nanci A. Understanding and controlling the bone-implant interface. Biomaterials 1999;20:2311–21.
[157] Falcinelli C, Li Z, Lam WW, Stanisz GJ, Agur AM, Whyne CM. Diffusion-tensor imaging versus digitization in reconstructing the masseter architecture. J Biomech Eng 2018;140:111010.
[158] Nalla RK, Kinney JH, Ritchie RO. Mechanistic fracture criteria for the failure of human cortical bone. Nat Mater 2003;2:164–8.
[159] Taylor D. Fracture mechanics: how does the bone break? Nat Mater 2003;2:133–4.
[160] Viceonti M, Olsen S, Nolte LP, Burton K. Extracting clinically relevant data from finite element simulations. Clin Biomech 2005;20:451–4.